Development and characterization of a high-spatial-temporal-resolution foot-sole-pressure measurement system

Abhinav Ashok Kalamdani

CMU-RI-TR-06-38

August 2006

The Robotics Institute
Carnegie Mellon University
Pittsburgh, PA 15213

Abstract

Humans and biped robots generate unique pressure distributions under their feet while standing and walking. These foot pressure distributions are very vital information to analyze balance and walking in humans, and to analyze and control the gait cycles in robots. This research work involved development of a measurement system for measuring foot pressures using the Tekscan's F-Scan foot pressure sensor, characterization of the system and conducting some experiments to evaluate the system and introduce some statistical measures to characterize the pressure maps. The multiplexer and interface electronics were designed and the data acquisition system was built. Then the system characterization including the single sensor and whole sensor calibration was done. The spatial resolution of the F-Scan sensor is about 25 mm², and the while scanning a single sensor element, the sampling time is about 0.3 ms, but sampling the complete sensor takes about 300 ms. So the issue is, there can be a trade-off between spatial and temporal resolution, reducing temporal resolution will increase spatial resolution and vice versa. The system was later evaluated using an in-house constructed simulation frame, which simulated the loading on an artificial leg, and generated unique pressure distributions for static and dynamic swaying of the leg. These pressure maps were analyzed using method of moments.

Contents

List of figures

1. Introduction

Analysis of bipedal gait has been a widely studied problem for clinical applications and as well for developing biped robots. Gait consists of kinematic and kinetic aspects. Kinematic aspects are attributed by motion of body segments. Kinetic aspects are attributed by the forces acting on the body. A huge component of the forces acting on the body are due to the contact of the foot with the ground during the support phases of the gait. The contact pressures and forces under the sole of the foot are important external features that affect the bipedal locomotion. The interesting components of the pressure maps are:

- Magnitude of the pressures
- Spatial distribution patterns of the pressures
- Dynamic variations in magnitude and distribution patterns

Well-known orthopedist Philip Lewin says, "The foot is the vital link between the person and the earth, the vital reality of his day-to-day existence." City College of New York anatomists Todd R. Olson and Michael E. Seidel write, "Because the sole is so abundantly supplied with tactile sensory nerve endings, we use our feet to furnish the brain with considerable information about our immediate environment", and yet even the most sophisticated humanoid robots are without sensation in their soles.

1.1. Foot pressures

It is important to understand the characterization of the foot pressures, that are observed in the humans and the robots. This section provides an introductory insight into the pressure distributions.

1.1.1. Foot pressures in humans

The foot pressures or also called as plantar pressures in humans, are characterized by the skeletal structure of the foot, and the distribution of muscles and flesh under the sole. The foot can be divided mainly into three parts – the forefoot, the midfoot and the hindfoot. The forefoot consists of toes and the frontal part. The midfoot consists of the mid support part and also the foot arch. The hindfoot links the midfoot to the ankle and also consists of the heel. In the static support phase the heel and the forefoot are in contact with the ground. And the pressures are distributed all along the foot. Typical left, right, anterior or posterior sways generate unique pressure distributions under the foot [16]. During the support phase of the gait cycle, the contact of the foot sole with ground is into three substages. When the heel touches down, until the foot is flat, is the initial touch phase. Then the stage between flat foot till heel lift off is the midstance stage and the third stage between heel lift off to the toe lift off is the propulsive stage [28]. This stage as we can infer is the stage with most stress on the foot. The pressures on the sole during single support phase usually vary from about 210 kPa to about 1015 kPa during the dynamic phases of walking [14].

1.1.2. Foot pressures in robots

Most of the present day biped robot feet are nonanthropomorphic, they are rigid blocks of metal, and very bulky. For example, the Bip robot's [21] design of the sole of the feet which are stiff are equated to the quasi stiff part of the human foot, that is the part from heel to the metatarsi (without toes). The foot is wide and heel is long, thus giving a good static stability. These are suited for slow and static walking, but not dynamic walking. The pressure distributions under such feet are quite trivial. They would have uniform distribution of pressure. In the case of dynamically walking robots, the feet are of shapes such as semi-cylindrical arch [29], and they have a soft heel. These feet roll on the ground during the support phase of the gait and the pressure distributions under the foot in such conditions look interesting. But again these are not very much anthropomorphic. If we want robots to walk like humans, then there is a need for a much human like design of the foot, and that would result in the foot pressure distributions as in the humans.

1.2. Significance of foot sole pressure maps

The pressure distributions are caused by the contact of the foot with the ground. The factors that affect the pressure distributions are:
- – Structure of the foot
- – Structure of the ground
- – Posture of the foot while standing and walking dynamically
- – Kinetics of the placement of the foot

1.2.1. Using pressure maps in humans

These factors differently influence the standing or walking functionality of humans or robots. Plantar pressure maps in the humans are used for diagnosis of foot related disorders [28], evaluation of gait and evaluation of balance in old aged people [16]. They are used for designing of better cushions under the sole in the shoes [10]. Now a days, with the advent of smart or ubiquitous computing, the pressure maps have been used for human computer interactions [23]. The posture of the foot and the dynamics of impact of the foot with the ground provide useful information about the person's mood and also can be used for entertainment industry. In development of lower limb prosthetics, the plantar pressure maps can be used for evaluation of the pressure distribution and also for control in active prosthesis, with electrical stimulations given to the motoneurons in the legs based on the force feedback from foot pressure sensors [30].

1.2.2. Using pressure maps in robots

In the bipedal robotics applications, there have been attempts to get tactile information which mention about measuring ground reaction forces [6], the Zero Moment Point (ZMP) and center of pressure [20, 21]. While in the nonanthropomorphic robot feet, where the feet are rigid and the pressure distributions are uniform, there is not much of useful information in the distribution, hence only the magnitudes are used. But in [15],

the authors discuss about using the tactile information for performing dynamic walking in the robots thus making them nonanthropomorphic. The dynamic walking needs a complete contour of the foot pressure distribution along with the magnitude of pressures. The pressure maps could also be useful to get the structure of the surface of the ground where the robot is walking. This could help significantly for getting a model of the terrain and planning the algorithms for balance control, and stable gait of the robot. The pressure map dynamics generated during walking are a cyclic process, and these dynamics can be used to control the walking cycle of the robots and also correct the disturbances the caused by abnormal walking or when uneven surfaces are encountered under the foot.

1.3. Measurement methods for plantar pressures

The methods for measurement have been classified by S. Urry in his review paper [14] into barefoot and in-shoe methods. All the methods mentioned below have been reviewed in [14].

1.3.1. Presently used methods

The in-shoe methods are all electronic, but not all barefoot are electronic. There are different methods in barefoot as well and few adapted for in-shoe. The figure 1.1. shows the classification. The methods that can obtain data under both static and dynamic conditions but cannot relate the temporal course of events are referred as cumulative methods. These are basically with passives devices that just show an approximate map of the foot pressures. The optical methods are pedobarography which uses total internal reflection and obtains a pressure map, photoelasticity which uses photoelastic material illuminated by polarized light, and textured mat cinephotography, which uses the textured rubber mat put under a glass plate, showing distortions caused by the pressures.
The electromechanical methods are more promising. The force plates which were segmented and in matrix forms, had strain guages as sensors which measured the strain on the metallic plates. The position of the placement of the foot, and managing the segments were a few problems with these. The capacitance mats were made with higher spatial resolution.

Smaller segments of capacitive sensors were made, and also the temporal resolution was higher, however cross talk between adjacent capacitors, lower bandwidth of operation and thick capacitors made them not very friendly to use. The piezoelectric multi-element plate was a feasible idea, but the expense in doing signal conditioning and high frequency interference were its problems. In the biped robots, the triaxial or 6-axial force transducers have been used in the feet for measurement of forces and moments since the feet have mainly been nonanthropomorphic [21]. The force sensitive resistors are the new type of sensors which are being used widely. The next section will discuss about them.

Plantar Pressure Measurement Methods

Barefoot Measurements

In-shoe Measurements

Cumulative Techniques

Optical Techniques

Electro mechanical Techniques

Contact area Force plate hybrids

Footprinting

Microcapsules

Foil pedobarography

Pedobarographs

Photoelasticity

Textured mat Cinephotography

Segmented & Matrix force plates

Capacitance mats

Piezoelectric multi-element plates

Force-sensitive resistor (FSR) arrays

Figure 1.1. Classification Plantar pressure measurement methods

1.3.2. Force Sensitive Resistors

The Force Sensitive Resistors (FSR™ is trade mark of Interlink Electronics, and the term FSR used in this document refers to FSR™) are the piezoresistive elements made by screen printing of piezoresistive ink on thin polymer film substrate. These are thin, they have good bandwidth, and manufacturing smaller segments is cheaper, hence they are preferred all along. The resistive methods have an advantage of lower noise interference, easier signal conditioning, and lower electronic cross talk. FSRs have been used as elements to build in-shoe sensory systems. The Tekscan has also made similar sensors probably with different construction techniques. However they show a similar response and characteristics as Interlink's FSRs.

1.3.3. Various data acquisition systems

The data acquisition system depends a lot on the application of the system. There have been umbilical data acquisition systems for measurement of plantar pressures [11]. But the disadvantage of being tethered did not lead to those being used a lot, however Tekscan does produce F-Scan system which is tethered. With the advent of wireless technology, there have been attempts to build wireless measurement systems [1] and also the Tekscan's F-Scan Mobile [27]. These do provide a good system but contain lot of

instrumentation on the shoes or the legs.

1.4. Project description

The goal of this project was to design, build, calibrate, analyze and use a measurement system capable of measuring the pressure maps under the foot over a good spatial resolution, a reasonable accuracy of measurement of magnitude of pressure in real time. The sensor chosen was Tekscan's F-Scan sensor with about 960 sensing elements called sensels. The advantages and drawbacks of this sensor are discussed in the later sections. Although the company sells a complete system with the sensor, data acquisition with or without tether, the system is expensive and not usable for custom built applications [1]. The F-Scan sensor however is available separately at low cost, but the non-availability of the detailed datasheet of the sensor made it possible to explore the various characteristics in detail. The main stages of the project were:
- a. Understanding the sensor characteristics
- b. Designing of the connector, and analog multiplexing
- c. Addressing scheme for sensor elements
- d. Signal conditioning and interface with microcontroller based ADC
- e. Data transmission, reception and visualization
- f. Calibration of the sensor on the whole and single sensel
- g. Characterization of the sensel
- h. Designing of experiments for using the sensor and analysis of the data

1.5. Organization of the thesis

This chapter has given an overview of the plantar pressures in humans and robots, use of these pressure maps, and the ways they have been measured. This thesis is aimed at studying the sensor and its usability and also investigating whether the designed measurement system is capable of being used for serious application. Chapter 2 discusses about the F-Scan sensor, its construction, its background information about the characteristics, and the places it is being used. The chapter also discusses about the pressure mapping system built by Tekscan. Chapter 3 provides the details of the hardware and the software designs. The details include the measurand, addressing scheme of the sensor, microcontroller and lower level softwares and then the user interface with data visualization. Chapter 4 contains the characteristics of the sensor, calibration of the measurement system, filtering. Chapter 5 is about the experiments performed to test the usability of the measurement system by performing different loading experiments and also does the analysis of the pressure maps obtained. Chapter 6 discusses about the interpretations of the complete project with conclusions.

2. Tekscan's F-Scan™ System

The F-Scan system (in this document F-Scan system means Tekscan's F-Scan™ System or F-Scan sensor means just F-Scan™ sensor) [27] provides the plantar pressure and forces acting on the feet of humans. The system uses paper thin re-usable sensors. The system instantly detects, displays and records the plantar pressure without disturbing the normal gait of the human.

2.1. F-Scan Sensor

The F-Scan sensor is a thin multi-laminate construction offering a high spatial resolution. The sensor belongs to the family of piezoresistive technology. It is a grid based sensor with a large number of smaller sensing elements called sensels which are equally spaced.

2.1.1. Sensing theory

The F-Scan sensor is resistive sensor whose electrical resistance is the result of its contact resistance of the pressure sensitive ink. The contact resistance R_c of the sensor can be described by:

$$R_c = \frac{C}{F} \qquad (2.1)$$

where C is the proportionality constant, F is the force applied normal to the contact surfaces. According to [23] C can be split into K, defining the roughness and elastic properties of the surfaces and ρ, which is the resistivity of the sensor. The authors of [23] also define the novel guage factor GF_c to characterize the force sensitivity of contact piezoresistive sensors:

$$GF_c = \frac{S_c}{F} = \frac{1}{C} \qquad (2.2)$$

where $S_c = 1/R_c$ is the contact's electrical conductance. The guage factor indicates the force sensitivity of the sensor. Higher the gauge factor, more sensitive is the sensor to changes in forces. With a constant elastic properties and surface roughness K, the lower the contact films' surface resistivity ρ, the larger is the guage factor. Hence to make sensors of different sensitivities, this property is used. Generally the conductances vary from zero for zero external forces to several $\mu Siemens$, for a maximum force which can be tolerated by the plastic substrate. The threshold force required to get the sensor into the operating region varies with the dimensions.

2.1.2. Construction of the sensor

The F-Scan is made of [13] an ultra-thin (0.16 mm [2]) double layer sheet. Each layer is

built on a flexible substrate made of a polyester film called Mylar®. These layers are laminated together with adhesive in the non-sensing area [23]. An electrically conductive ink is printed on the film and coated with a pressure sensitive, resistive ink such that the parallel rows of electrodes on the top layer face parallel columns of electrodes on the bottom layer through the resistive ink. The screen-printing technology is used to deposit all the material on the sheets. The distance between two parallel rows or columns is about 5 mm. The intersections of the rows and columns construct the pressure-sensing cells or the sensels as shown in the figure 2.1. The contact of the row and column at the sensel spot, at the micro-structural level is as shown in figure 2.2., show a lot about the way the sensor works.
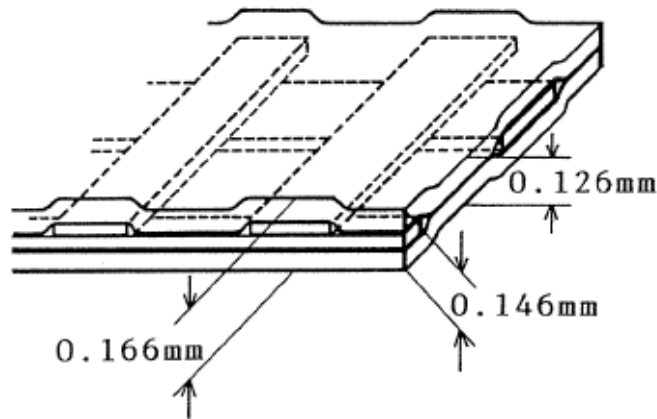
Figure 2.1. Section of the sensor film. [2]

Figure 2.2. Microstructure of the resistive ink contact surface [13]

In the figure 2.2., A is the back surface of the top layer, D is the back surface of the bottom layer. B and C are the resistive ink surfaces of the top and bottom layers respectively. The electrical resistance is affected by the contact of the B and C surfaces. The resistive ink is of fixed resistivity, but has changing surface roughness and elastic properties and this results in variation of sensitivities of the sensels of the sensor.

The geometry of the film is in the shape of the sole of the shoe, such that it can be placed inside the shoe under the foot for in-situ measurements. The signal bus terminates near the center of the array, so that the edges can be trimmed to fit a particular shoe size; the white lines in the right picture of figure 2.5, shows the boundaries along which the sensor can be trimmed. Figure 2.3. shows the shape of the sensor and also the arrangement of the grids of the rows and columns. The sensel is a square with side of 5.08 mm and area of 25.80 mm². Comparing the sensel area to quantity of sensitive area of the human skin which is 625 mm² [23], the F-Scan sensor oversamples the pressure distribution.

However the sampling can be reduced if needed for a particular application. The sensor film totally contains about 960 sensels. There are 60 rows and the columns are divided into lower and the upper sets a shown in figure 2.4. A set contains 18 columns and B set contains 21 columns. The electrical connection is such that all columns have unique terminals, but only a few rows have unique terminals, otherwise two rows are connected in parallel, thus effectively giving only 36 row terminals. With proper multiplexing of the connections, it is possible to isolate the individual sensels for measurement.
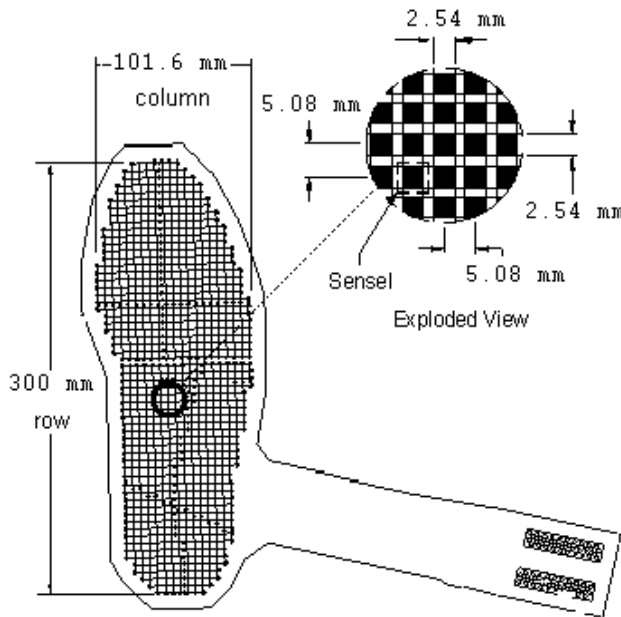
Figure 2.3. The geometry of the sensor [27]   Figure 2.4. Column arrangement
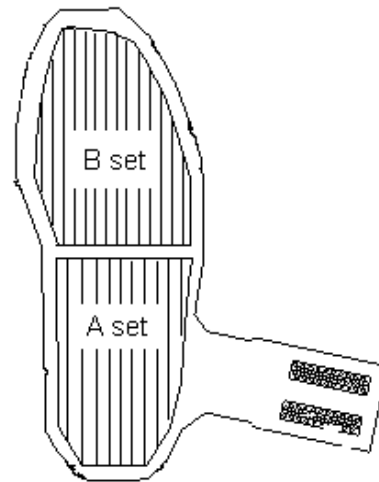
2.1.3. Characteristics of the sensor

The F-Scan sensor has been mainly used for clinical applications since mid 1990s. And researchers have also done validation tests of the sensor with different experiments and tried to characterize it in detail.

The advantages of the sensor are it is very thin, simple and robust for usage. The dynamic response of the sensor encourage dynamic measurements and the spatial resolution make the sensor good for measuring dense pressure maps. The conductance versus the pressure curve of the sensor is linear. The section 3.1.1 discusses the linearity of the sensor. However, there are a few disadvantages of the sensor. According to [14], the sensor undergoes delamination after 30 gait cycles of usage. The validation experiments done by [13] show that the sensor responds not only to the applied external pressures, but is also influenced by surface contact hardness conditions, creeping of coated resistive ink under pressure and temperature.

Figure 2.5. F-Scan sensor film. The left picture shows the rows of the film and right picture shows the columns.

Looking at the microstructual level, from figure 2.2., we can learn that the surface roughness in the sensels is different at each sensel, and this leads to inconsistency in the sensitivity, hysteresis, and also low accuracy among different sensels. Hence [5] says that the sensor system does not yield repeatable measurements and so F-Scan is not suitable for absolute accuracy. Another major setback to the sensor is the time drift [6]. The sensor conductance increases with increase in temperature, but the amount of increase is low within 30°C [13].

The surface contact hardness on the sensor was studied [13]. It was noted that the sensor showed best results with soft-soft contact surface, so it was recommended in [13] to use soft contact surfaces.

2.2. Tekscan's F-Scan monitoring system

The Tekscan has produced the complete monitoring system for measurement of foot pressure using the F-Scan sensor. The basic F-Scan system is a tethered, USB based data acquisition system, with all the electronics in a box that is attached to the sensor. There are other versions wherein the communication is wireless. Figure 2.6. shows the way the instrumentation fit on the leg. The sampling rate of the whole sensor of 960 elements is 165 Hz. So it would give a very dense amount of information about the dynamic pressure maps. The multiplexing electronics used by Tekscan's system to scan the arrays of the

sensels is as shown in figure 2.7. [23].

Figure 2.6. Fitting of the instrumentation of F-Scan system on the leg [27]
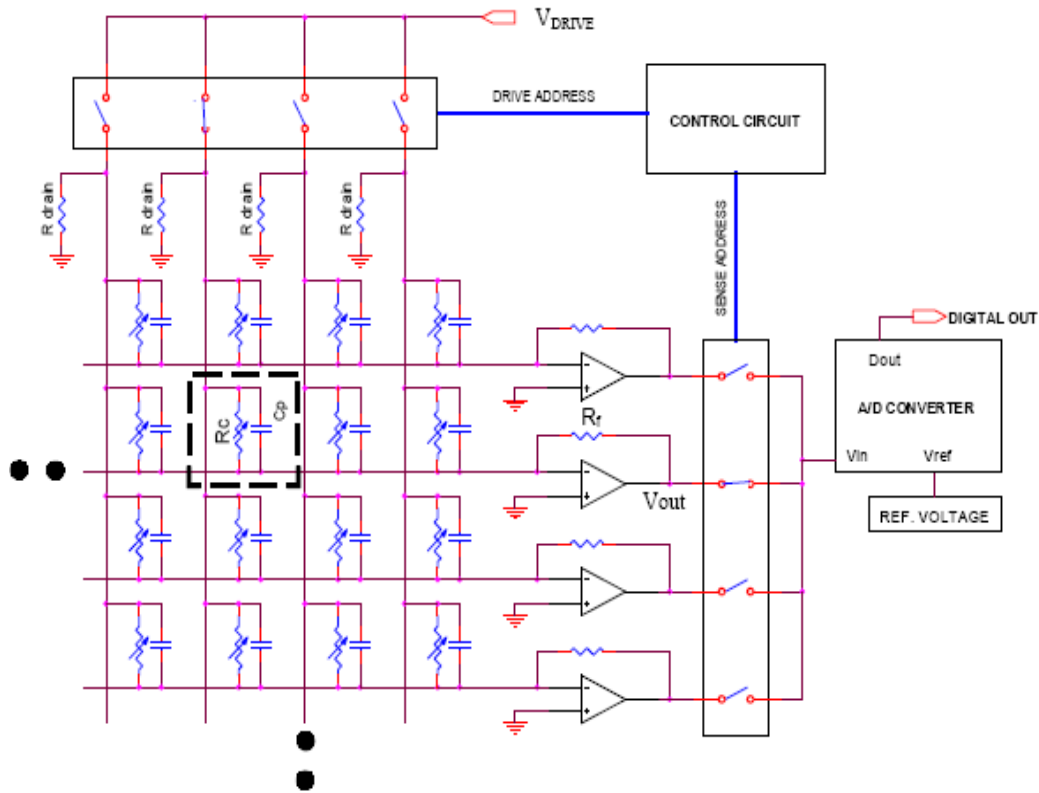
Figure 2.7. Multiplexing electronics of Tekscan's F-Scan system [23]

The control circuit selects the row and column and the sensel would be activated and the voltage at the Vout is captured by the ADC. This Vout is proportional to the sensor conductance S_c :

$$V_{out} = -V_{drive} R_f S_c$$

The sensor is calibrated in terms of pressures by using pneumatic calibration device [27]. And also in the view of not good accuracy, the sensor is recalibrated in-situ, by the subject's weight [2]. However [5] says that the F-Scan calibration protocol is inaccurate.

18

The analysis software of the system offers a clear 2D and 3D visualization of the pressure maps in real time and of recorded data. The dynamic range of the pressures is shown by the colormaps. The software also gives an information about the center of pressure and its trajectory along the gait cycles. The force and pressure curves are also visualized. It also shows the force integrals over time (impulse). However there are additional packages which provide much more analyses facilities for example, the TAM™ is the timing analysis module, which analyses the phases of the gait cycle, CoM'nalysis™ analyses the body's center of mass and energy efficacy, and Video Synchronization™ is used to make the video of the dynamic pressure maps. Figure 2.8 shows the screenshot of the visualization software.
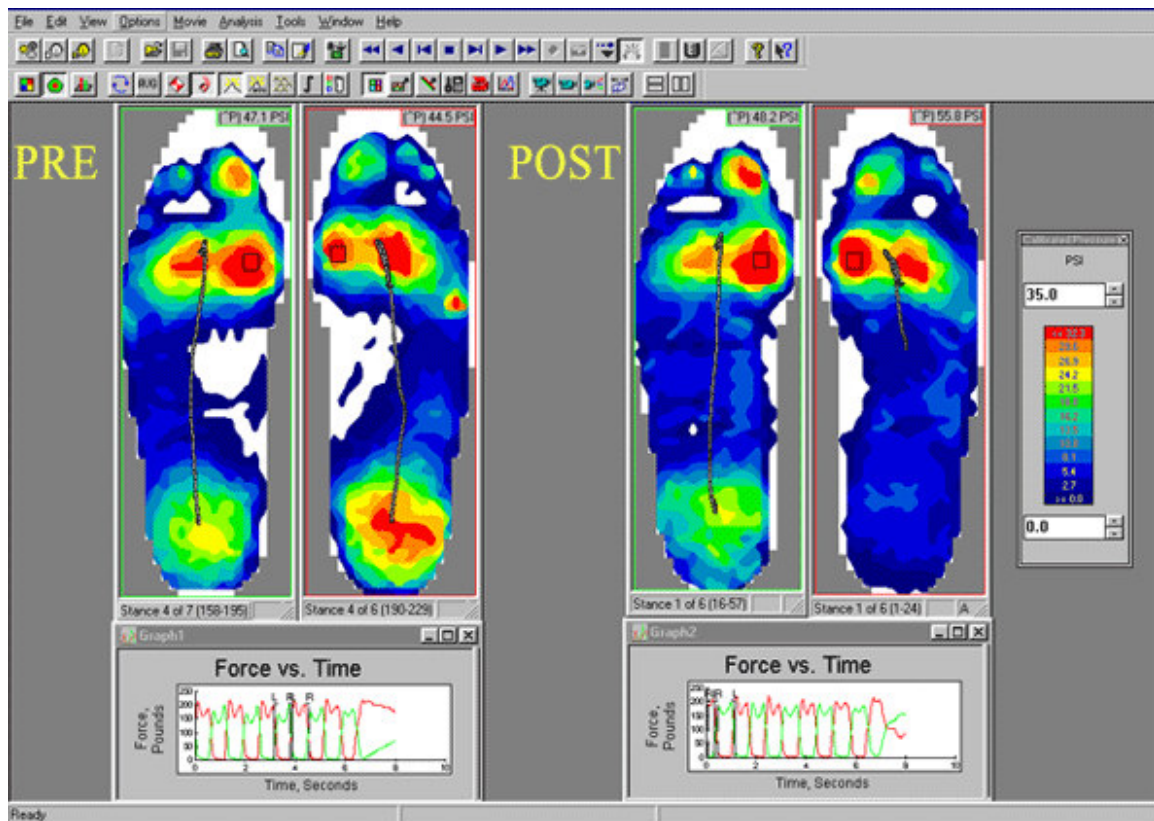
Figure 2.8. Screenshot of the software used for visualization in F-Scan system

3. Hardware and Software

The rationale that is followed for the design of the hardware and the software is as described in the section 1.4 of this document. The figure 3.1 shows the architecture of the whole system as described in 1.4. The process is triggered by the Matlab user interface which commands the EXE to communicate with the micro-controller, and requests the micro-controller to start data acquisition. The micro-controller then configures the ADC and sends the specified sensel address on the digital I/O which selects the particular row and column of the F-Scan sensor using the analog multiplexer. The interface electronics drives the the sensor element and produces a voltage corresponding to the resistance as shown by the sensel, which is digitized by the ADC. The micro-controller then sends the digitized data through the serial communication to the PC. This cycle carries on, sequentially scanning the sensor. First and foremost task is to get the response curve of the measurand which is the resistance or the conductance of the individual sensor element.
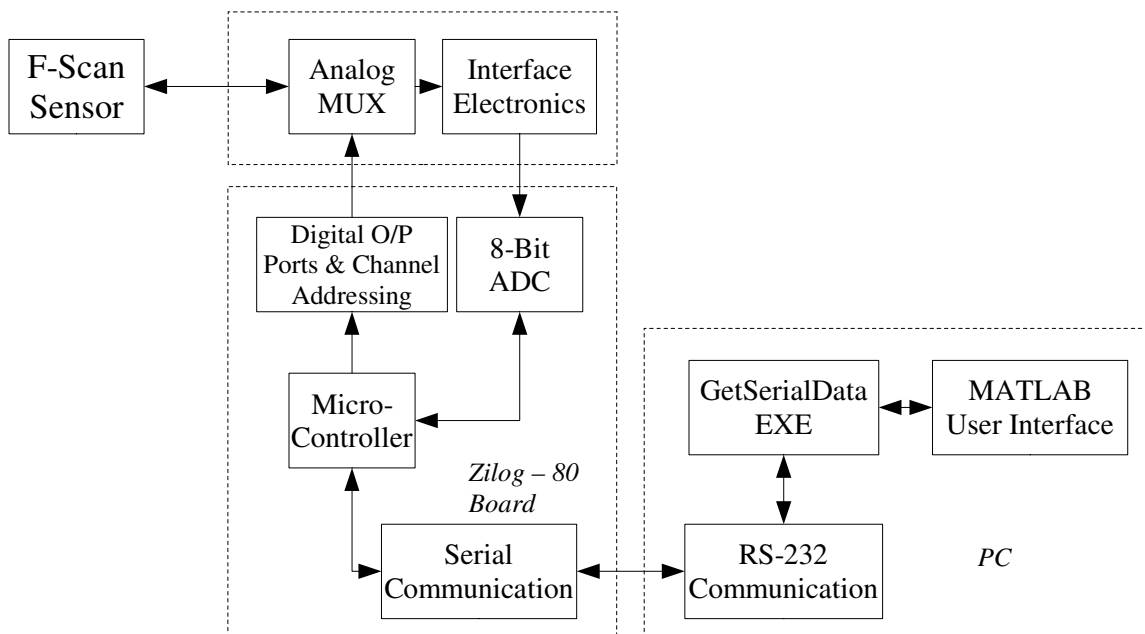
Figure 3.1. Block diagram of the system

3.1. Measurand and Interface Electronics

3.1.1. Measurand

The section 2.1.1. gives a clear relationship of the measurand that is the pressure and the resistance or conductance of the sensor element. An experiment was carried out on a sensor element which provided the response curve of resistance versus the pressure that was being applied. The loading was applied by placing 4 cubical rubber pegs, each having the surface area same as that of the sensor element 25.80 mm², on the sensor points and then placing the loads on a plate over the 4 pegs. The pressures applied were from 0-537

kPa by placing 0-5.7 kg of dead weight on the plate. Figure 3.2. shows the measured resistance versus pressure response. The conductance versus pressure curve of the sensor shows almost a linear response. And recalling the equation 2.2. the guage factor or the sensitivity of the sensor can be found. The relation is given by

$$S_c = GF.P \qquad (3.1)$$

where P is the pressure in kPa. A least squares straight line fit to the data is conveniently found by treating the data points of conductance versus pressure curve in figure 3.2 (right), as elements of vectors $\mathbf{P}$ and $\mathbf{S_c}$ (each 12 data points X 1 column), from which

$$\mathbf{P}_{(12\times1)}.GF = \mathbf{S}_{\mathbf{c}(12\times1)} \qquad (3.2)$$

and the GF is found by

$$GF = (\mathbf{P}^{\mathrm{T}}\mathbf{P})^{-1}\mathbf{P}^{\mathrm{T}}\mathbf{S_c} \qquad (3.3)$$

The guage factor found was $GF = 5.29 \times 10^{-7} S\, kPa^{-1}$.
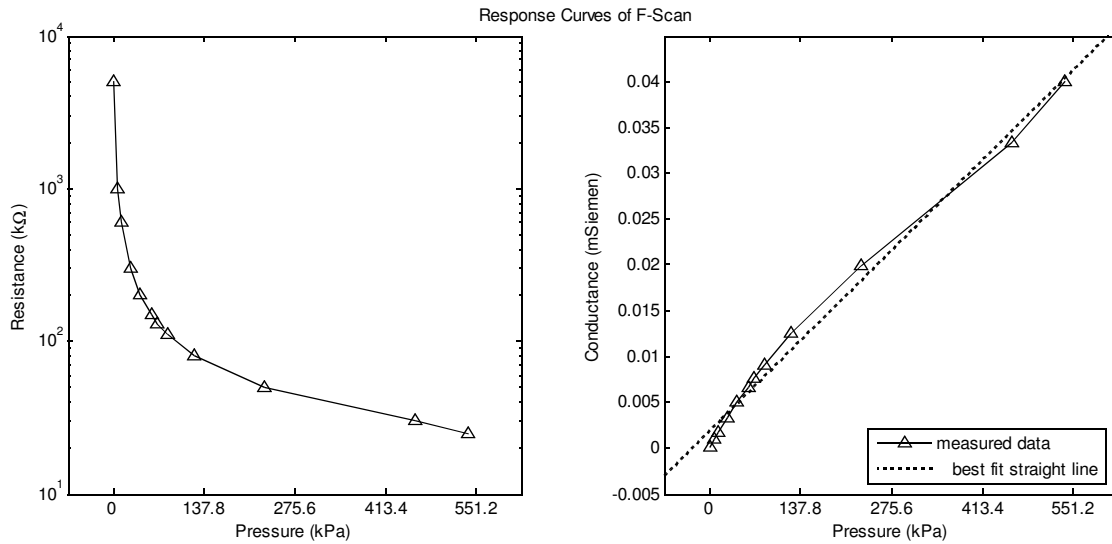
Figure 3.2. Response curves of the sensor element

3.1.2. Interface electronics

The circuit design for interfacing the resistive sensor to the ADC will influence the dynamic range of the sensor. Using op-amps would introduce spurious effects of offset especially when we are using the ADC with lower reference voltage. The circuit as used by Tekscan shown in figure 2.6, would certainly give a good response, but as is seen, there is a need for either 36 or 39 op-amps with very low offsets. This increases the complexity and the costs. Hence the circuit design given by [1] has been implemented. This design is with just a voltage divider succeeded by an emitter follower, using an NPN

transistor as shown in figure 3.3. The relation between the output voltage V_{out} and the resistive element R_{sen} is given by

$$V_{out} = \left(\frac{R_{sen}}{R_1 + R_{sen}}\right).V_{cc} - 0.42 \qquad (3.4)$$
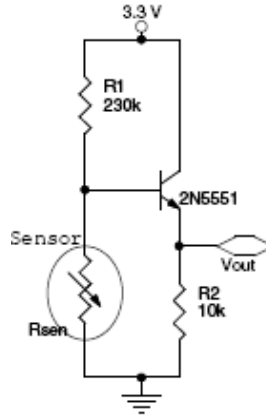
Figure 3.3. Interface circuit for resistive sensor

where V_{cc} is 3.3 V, the factor 0.42 V is the base-emitter voltage across the transistor. This circuit will give an output voltage that decreases with increase in pressure. The ADC of the Zilog – 80 board has a reference voltage of 2.25 V. Hence the V_{out} should give 2.25 V at the threshold pressure and should give 0 V at the maximum pressure. Using these conditions the resistance R_1 of the circuit was designed to be 230 kΩ. This gave a response as shown in the figure 3.4. From the response curves, we see that the voltage range is well within the reach of the voltage range for the ADC i.e. 0-2.25 V and cross referring the figure 3.2., the sensor response to pressure shows that the pressure input range is 0-551 kPa. Now that the interface electronics is designed for a large range of pressure inputs, the sensor has to be addressed properly.

3.2. Scheme of addressing the sensor and multiplexer design

3.2.1. Matrix of sensor elements

The sensor matrix is made up of 60 rows and two sets of columns, A and B, with 18 and 21 columns respectively. The figures 3.5 and 3.6 show the arrangement of these rows and columns. The sensor element is selected by its unique row and column. This forms the resistive sensor. Hence, to read the complete sensor, each of the sensor elements has to be addressed sequentially and each of this resistive sensor has to be "connected" to the interface circuit as shown in figure 3.3. There is a change in the addressing of the rows. Rows 1 to 8, 43, 48, 53 and 58 have unique terminals, but in the case of rest of the rows, two rows share a single terminal. So, if one terminal is addressed then two rows would be selected. That is the reason why 60 rows can be addressed by just 36 terminals. However in case of columns, every column has a unique terminal. This architecture needs two

multiplexers that will select the specified row and the specified column respectively. The next section discusses this multiplexer design.
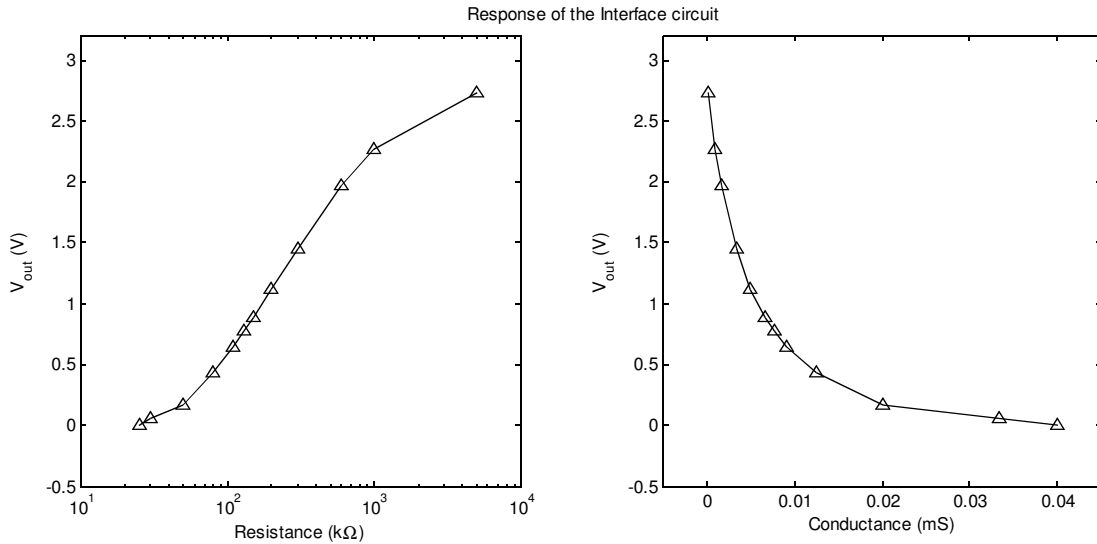
Figure 3.4. Response of the interface circuit
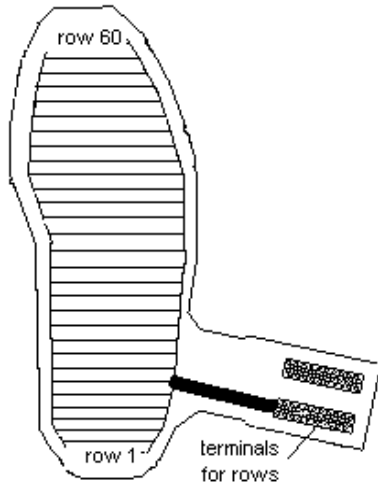
Figure 3.5. Arrangement of rows
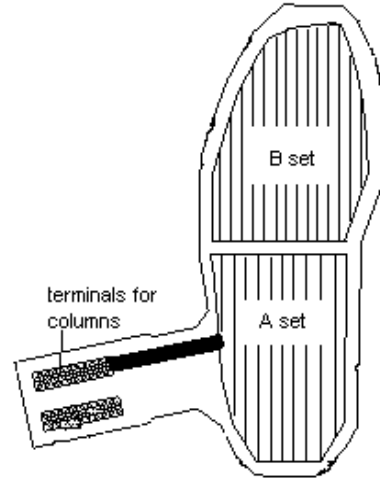
Figure 3.6. Arrangement of columns

3.2.2. Analog multiplexers

The selection of the row and column will select the specified sensor element which will be interfaced to the voltage divider circuit. Since the signal that would flow through the multiplexer is analog, there is a need for the analog multiplexer design. There are 36 terminals for rows and 39 for columns. So two 40-channel multiplexer sets are used for the addressing of the rows and columns. Each multiplexer set consists of two ADG406 16-channel and two ADG428, 8-channel analog multiplexers manufactured by Analog Devices as shown in the figure 3.8. The row or column terminals are connected to the two 16-channel and one 8-channel multiplexers which form the 40-channel selectors. The

outputs of each of these three multiplexers are connected to the channels of the second 8-channel multiplexer. These 40 channels are selected by 6-bit address lines as described in figure 3.7.
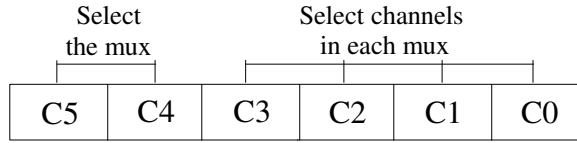
Figure 3.7. Structure of the address passed to the multiplexer set

The two sets of the analog multiplexers are used to address the whole sensor and the outputs of each of it are connected to the interface circuit as shown in the figure 3.9. The two 6-bit addresses will select the row and the column and the sensor element is now connect to the interface circuit. Hence the V_{out} of the circuit will give the value of the pressure exerted on that specific sensor element. When all the sensor elements are scanned similarly by addressing the multiplexers, the pressure on all the sensor elements is measured. The scheme of scanning can be custom designed. The schemes that were tried were sequential row-wise scanning and also random scanning. The scheme of random scanning seemed to be better since it avoids delay in scanning the opposite side of the foot during the dynamic operations. Other schemes that could be tried out are sparse scanning to avoid oversampled pressure maps or smart scanning which can involve the dynamics of the motion.
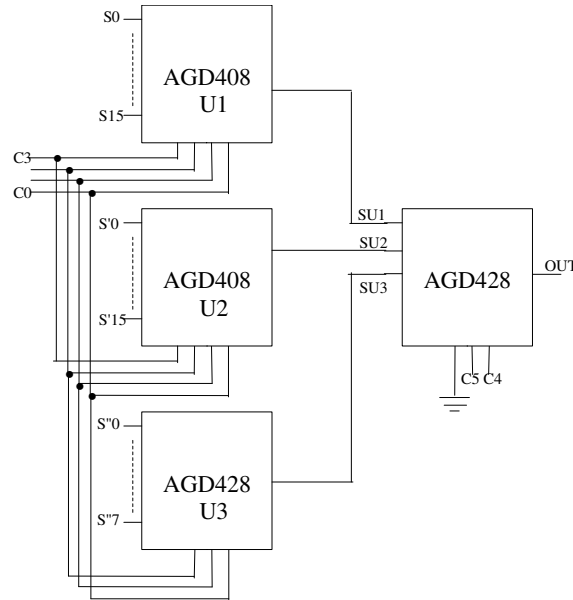
Figure 3.8. Design of one set of analog multiplexer for either the row or column, C0...C4 are address lines, S0..S15, S'0..S'15 and S"0..S"7 are signal lines. SU1, SU2, SU3 are intermediate partially selected signal lines
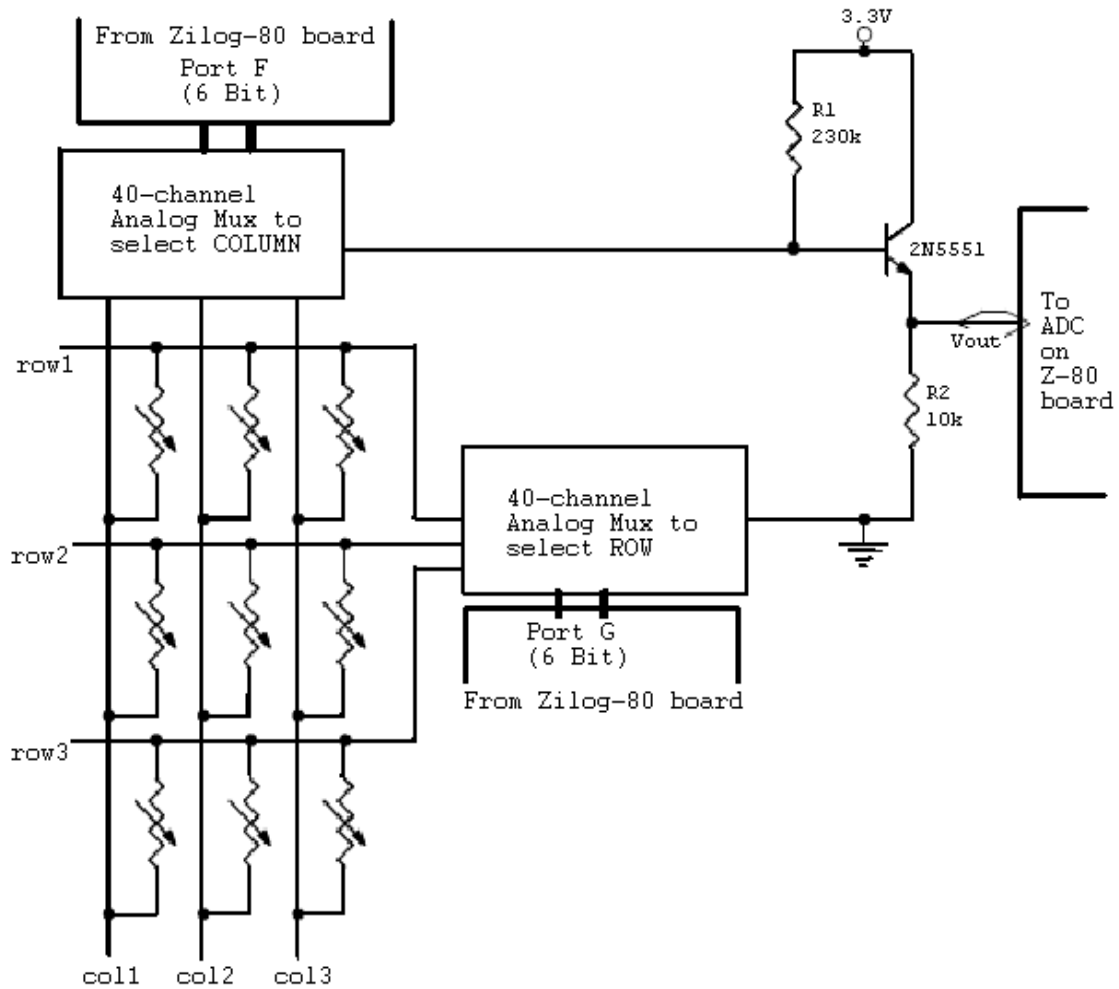
Figure 3.9. Sensor, analog multiplexers and interface circuit

3.3. Micro-controller interface and low level software

The Zilog-80 board was used for the low level data acquisition. The micro-controller used was Z8F6403xxx. This is a high end micro-controller running at 18.432 MHz and has 64 kB of flash memory, 4kB of RAM, 12-channel 10-bit ADC, timers, serial communication, 60 digital I/O pins and many more features. The micro-controller and other peripherals are on the Z8 Encore evaluation board with a feature for serial on-chip debugging. The Z8 Encore IDE is fully loaded with all the debugging features with a C-compiler, hence making it easy to implement the software.

3.3.1. On-board ADC

As mentioned, the micro-controller has an on-board 10-bit ADC with an analog multiplexer for 10-channels. However, for this project we used a single channel since in actuality there is just one ADC, and instead of using the on-board analog multiplexer, we used an external multiplexer. The on-board ADC is a sigma-delta ADC. So it offers high

resolution, low digitization noise, and suitable for low frequency signals. Hence it is good choice for the precision measurement systems. The characteristics of the ADC with 18.432 MHz clock frequency are [26]:

- – Resolution : 10 bits
- – Input signal bandwidth : 3.5 kHz
- – Reference Voltage : 2.25 V
- – Sampling rate : 72 kHz
- – Mode of operation : Single shot or continuous conversion
- – Continuous conversion time : 14 μs
- – Input impedance : 3.0 kΩ
- – DC offset error : 15 mV

Since the output voltage of the interface circuit is already designed to be from 0 – 2.25 V for useful pressure measures, and since there is also a voltage follower, connecting the output of interface circuit directly to the ADC pin is not an issue. It is connected to the ALG0 pin which is also shared by PortB0, but the pin can be configured for analog input. The ADC is operated by the Direct Memory Access (DMA), whose controller automatically initiates data conversion and transfers the data from the ADC channel to the specified RAM location. The details of the implementation of the ADC are discussed in the next section.

3.3.2. Low level software

The low level software for the micro-controller is designed for time optimal data acquisition and transmission to the PC. The figure 3.10 shows the flowchart of the software that is loaded in the micro-controller. According to the flowchart, the system will scan the sensor completely once. This starts by getting a command in the form of character 'a' on the serial communication (UART) module. The PC sends this command and waits for the data. Once the command is received, the DMA ADC and interrupts are initialized. Then the interrupt service routine is activated; this will recognize the interrupt from DMA controller and will set the flag saying the data is ready, and then the ADC conversion is started. The starting character 's' is sent over the UART indicating the header of the stream of the data, and then the sensor scanning starts. The ADC is read, then conversion is stopped, and only upper 8-bits are transmitted over UART since the serial communication is configured for only 8-bit data. Knowing about the behavior of the sensor, and its bad repeatability for higher resolution, we decided to use only 8-bits for representing the digitized voltage. Once the data are sent, the next sensor element is selected by sending the specified address on the ports F and G which will drive the analog multiplexer to select the specified row and column. When all the sensor elements (number of sensor elements specified by NO_SENSEL) are scanned, the ending character 'e' is sent over the UART. This completes the transmission of the data from the micro-controller to the PC. This process can be repeated by simply sending the character 'a' from the PC, which will command the microcontroller to start the scanning process. Since the characters "s" and "e" form the header and footer of the data, and the exact number of bytes forming the data is known, it is easy to distinguish between these header and footer characters and the data.

It has to be noted here that the interrupt service routine takes care of multitasking. The conversion is started immediately when the previous completion interrupt occurs. And while the conversion is going on, the previous data are loaded into the UART transmit buffer, so that simultaneously the data are transmitted. This ensures low delays in the whole scanning. The scheme of addressing the sensor as discussed earlier is carried out by a separate function, which has a lookup table of the addresses at different bytecounts. The reason for this lookup table is because of the random scheme of addressing, or as discussed, the scheme of addressing can be adopted accordingly for necessary resolution. The bytecounts are basically the indices of the sensor elements. These drive the lookup table and send the specific address on the ports. The same protocol is used at the PC to decode as to which index belongs to which sensor element location (row and column).

3.4. User Interface

The PC side of the system is based on, an executable developed using Visual C++ for interacting with the serial port of the PC, and the Matlab platform which will do the processing and display of the data received in real time.

The executable GetSerialData.exe is modified from a publically distributed program called ADRTEST [http://www.ontrak.net/mfc.htm]. This executable accesses the serial port, sends the command character 'a' and then waits for receiving the data from the Z-80 board. Once all the data are received with a terminating character 'e', the data are written to a binary file.

The Matlab module reads that binary file and collects the data, and using the protocol that was discussed in section 3.2.2 in terms of addressing the sensor, the data indices are decoded and the proper sequence of the data is obtained. Using the lookup table which specifies the indices of the data and the location of the sensor element on the sensor, the pressure map is written into a matrix and displayed as an image with a colormap indicating the dynamic range of the voltages in terms of unsigned 8-bit integers. Figure 3.11 shows the display of the raw data as received from the microcontroller. Note that the range is from 0-255 and the locations of the pixels are in accordance to the locations of sensor elements on the sensor film. The pressure map is refreshed with the new data hence showing the visualization in real time with a lag approximately of 300 ms. There are also options for storing the data. Whatever data processing is to be done, it will be done before displaying the data within the function. The following section discusses the characteristics of the measurement system and data processing.

```
                            ┌──────────────┐
                            │    Start     │
                            └──────┬───────┘
                                   │
                        ┌──────────▼──────────┐
                        │ Initialise UART, Ports │
                        └──────────┬──────────┘
                                   │
          ┌───────────────────────┤
          │            ┌───────────▼──────────┐          ┌──────────────────────────┐
          │            │      Read UART       │◄────────►│ UART recieves data from PC │
          │            └───────────┬──────────┘          └──────────────────────────┘
          │                        │
          │            ◄─────◇ Is 'a' ◇
       NO │              NO  ◇ recieved? ◇
          │                        │ YES
          │            ┌───────────▼──────────────┐
          │            │  Initialise DMA ADC for  │
          │            │  - continuous conversion │
          │            │  - single channel        │
          │            │  - with high priority interrupt │
          │            └───────────┬──────────────┘
          │                        │
          │            ┌───────────▼──────────────┐   ┌──────────────────────────────┐
          │            │ - Set DMA vector interrupt│   │ Interrupt Service Routine (ISR) │
          │            │ - Enable interrupt        │──►│ checks for source of interrupt and │
          │            │ - start conversion        │   │ if the source is DMA then it sets │
          │            └───────────┬──────────────┘   │ data_ready = 1                  │
          │                        │                    └──────────────────────────────┘
          │            ┌───────────▼──────────────────────┐
          │            │ Transmit 's' on UART and set bytecount = 0 │
          │            └───────────┬──────────────────────┘
          │                        │
     ┌────┼────────────────────────┤
     │    │            ◇     Is         ◇          NO      ┌──────────────────────┐
     │    │            ◇ bytecount < NO_SENSEL ? ◇────────►│ Transmit 'e' on UART │
     │    │            ◇              ◇                     └──────────┬───────────┘
     │    │                        │ YES                              │
     │    │            ◇     Is         ◇      NO              ┌───────▼───────┐
     │    │  ◄─────────◇ data_ready == 1 ? ◇                  │     Stop      │
     │    │            ◇              ◇                        └───────────────┘
     │    │                        │ YES
     │    │            ┌───────────▼──────────┐
     │    │            │ - set data_ready = 0 │
     │    │            │ - disable interrupts │
     │    │            │ - stop conversion    │
     │    │            └───────────┬──────────┘
     │    │                        │
     │    │            ┌───────────▼─────────────────────┐
     │    │            │ Read upper 8-bits of the converted data │
     │    │            └───────────┬─────────────────────┘
     │    │                        │
     │    │      ┌─────────────────▼─────────────────────┐   ┌──────────────────────────────┐
     │    │      │ Send next address on Ports F & G to select next sensel │◄►│ Get bytecount and send the address from │
     │    │      └─────────────────┬─────────────────────┘   │ the lookup table               │
     │    │                        │                          └──────────────────────────────┘
     │    │      ┌─────────────────▼─────────────────────┐   ┌──────────────────────────────┐
     │    │      │ Load the UART's transmit buffer with   │◄►│ UART module takes care of      │
     │    │      │ converted 8-bit data and enable transmit │  │ transmission after transmit bit is enabled │
     │    │      └─────────────────┬─────────────────────┘   └──────────────────────────────┘
     │    │            ┌───────────▼──────────┐
     │    │            │ - Start conversion   │
     │    │            │ - enable interrupt   │
     │    │            └───────────┬──────────┘
     │    │            ┌───────────▼──────────────────┐
     │    │            │ Set bytecount = bytecount + 1 │
     │    │            └───────────┬──────────────────┘
     │    └────────────────────────┘
     └─────────────────────────────
```
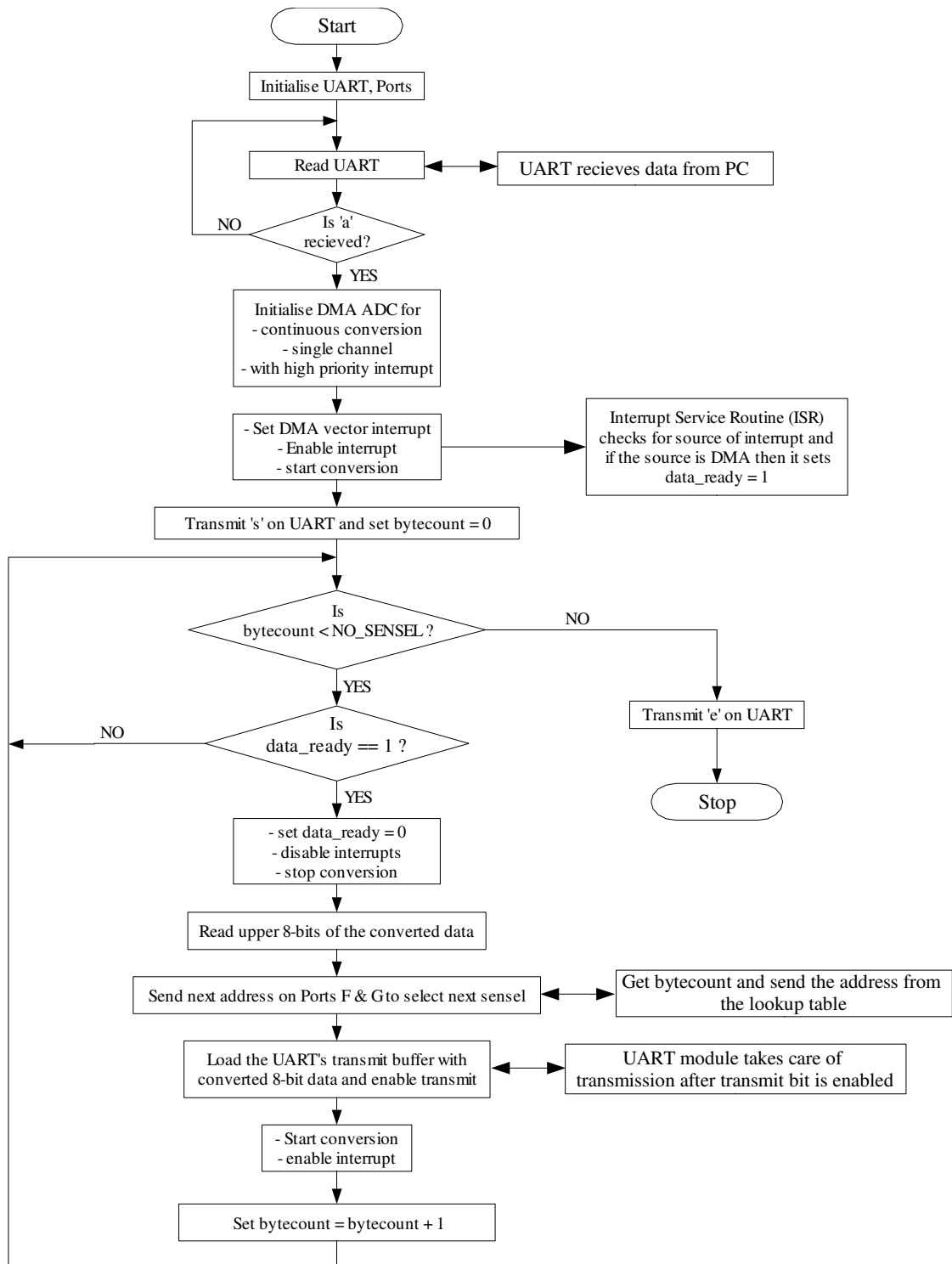
Figure 3.10. Flowchart of the low level software running on the Zilog microcontroller for scanning the sensor completely once
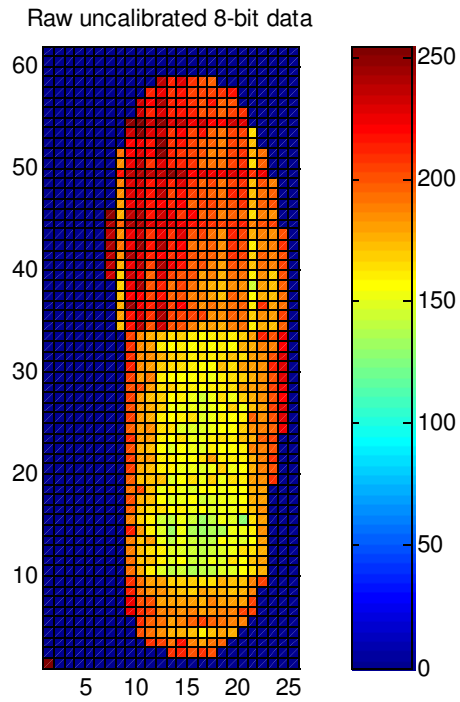
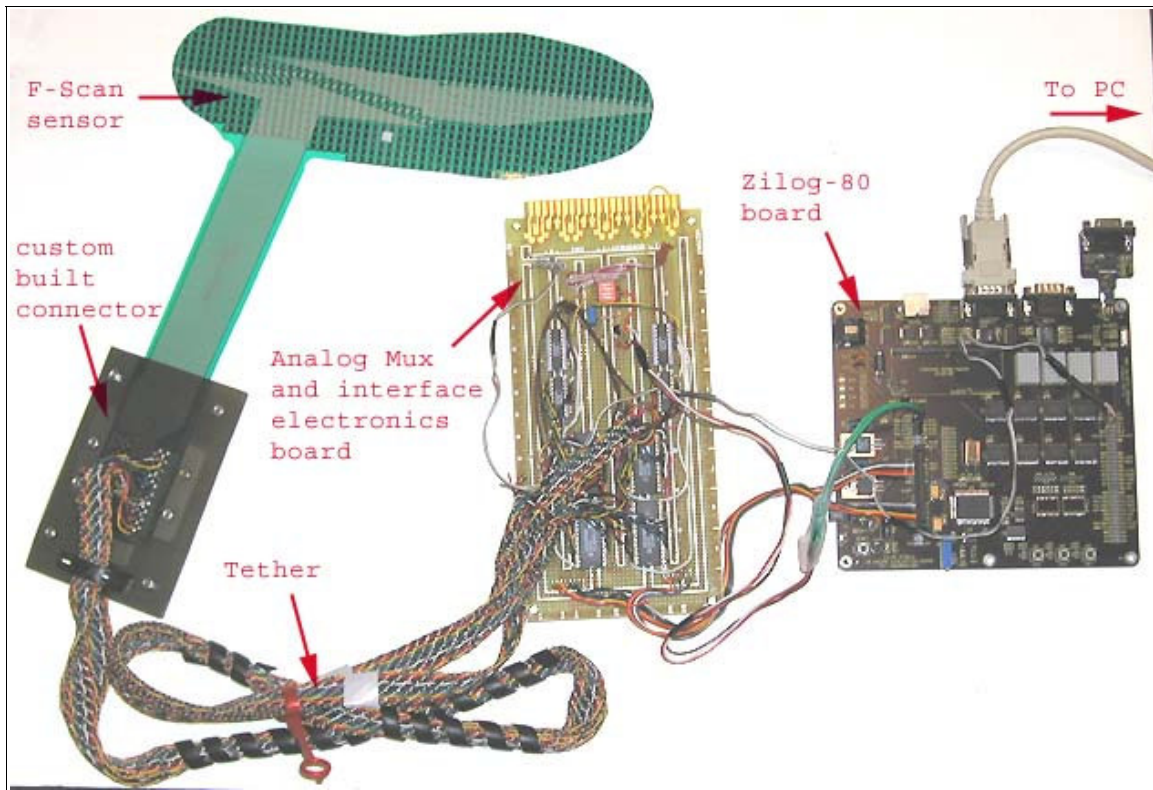Figure 3.11. Visualization of the raw data as received from the micro-controller

Figure 3.12. The measurement system hardware, with the sensor, and the other electronics

4. System characterization

Now that the measurement system is built, it needs to be characterized and the data needs to be processed for using it in various applications. The first task is to calibrate the sensor within the specified range of operation. The next task is to measure the characteristics of a single sensor element and also the complete sensor. The last part is to make the data useful for processing, and spatial filtering is discussed about.

4.1. Calibration of single sensor element

Calibration is the method by which the measurement system's output is related to an engineering unit. The section discusses about the method for loading a single sensor element and obtaining the calibration curve for the element. Then the calibration curve and relationship with the transfer function is shown and the curve fitting is discussed.

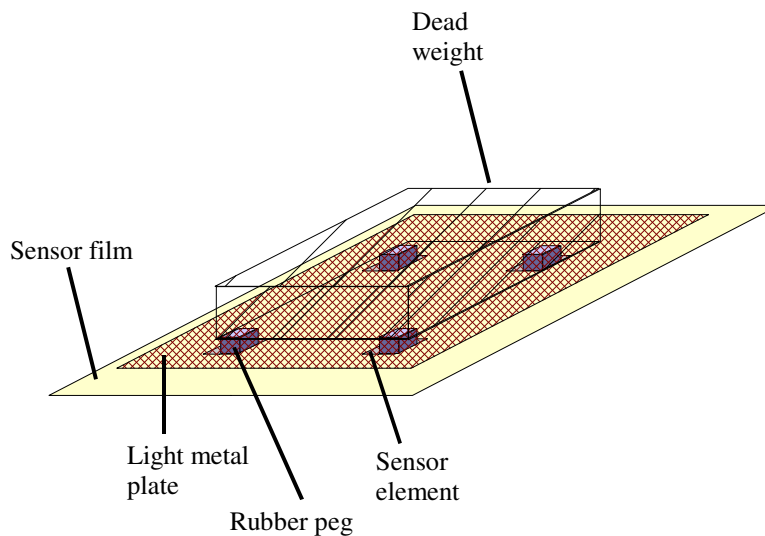### 4.1.1. Loading a single sensor element

Figure 4.1. Loading method for the sensor

The sensor elements form the active region and the area of the sensor element has to be fully covered by the loading body. This will ensure uniform distribution of load over the area of the active region. Sharing the load by neighboring sensor elements might average out the loading and also the problem of neighborhood distortion (will be discussed in 4.2.6) will rise giving erroneous results. Hence the best choice would be to use small cubical pegs with surface area same as the sensor element area.

The next issue is with the material to be used for the pegs. According to [13], the sensor gives best results when the soft material is used to create contact with the sensor. So rubber pegs were used for loading. As shown in the figure 4.1, there were four pegs which were placed on distant sensor elements, and a light metallic plate was placed over

the four pegs. On the light metallic plate the dead weights were placed. In our experiments, we used the ceramic tiles for loading as dead weights. Each tile was 1.57 kg. The total area in contact with the sensor was about 152.26 mm². The maximum load that was placed was 7.85 kg by five tiles, thus exerting a maximum pressure of about 503 kPa. There is a need to take care about not getting the system saturated for getting the calibration curve, which is why only 503 kPa was exerted.

This experiment was carried out after conditioning the sensor [24]. The conditioning helps to reduce the effects of drift and hysteresis. It is done by placing higher load than the range and then allow the sensor to stabilize and then unload it. This is done 3-4 times before calibrating it. So conditioning was done by placing about 9.42 kg i.e. six tiles on the plate. The sensor was loaded statically and the digital reading was obtained for four sensor elements. The figure 4.2 shows the calibration data that was recorded for 2 sensor elements. And it is distinct that though the readings for the two sensor elements were different slightly, the curve profile was consistent. Researchers, previously having recorded the behavior of the sensor elements, say that they differ in their behavior due to the manufacturing drawbacks and non-homogeneity in the material [22]. The digital reading range for this is from 0 – 255 for pressures from 0 – 503 kPa.
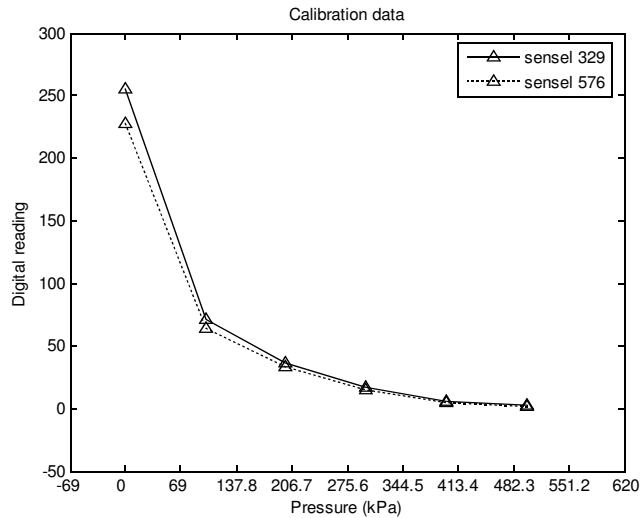

Figure 4.2. Calibration curves for two sensor elements

4.1.2. Computing calibration parameters

There is a need to derive the transfer function of the measurement system for calibration. Starting from equation 3.4, and using the equation 3.1, the output voltage can be written as

$$V_{out} = \left(\frac{1}{R_1 G_{sen} + 1} \right) . V_{cc} - 0.42 = \left(\frac{1}{R_1 GF P + 1} \right) . V_{cc} - 0.42 \qquad (4.1)$$

where G_{sen} is the conductance of the sensor element in S, GF is the guage factor in S/kPa, P is the pressure exerted in kPa and 0.42 V is the base-emitter voltage of the

transistor. Writing the equation for pressure as output and voltage as input, will give the transfer function of the measurement system needed for calibration. Equation 4.2, states this transfer function.

$$P = \frac{-\left(\dfrac{1}{R_1\,GF}\right)V_{out} + \left(\dfrac{V_{cc}-0.42}{R_1\,GF}\right)}{V_{out}+0.42} = \frac{-\left(\dfrac{1}{R_1\,GF}\right)D + \left(\dfrac{255\,(V_{cc}-0.42)}{2.25\,R_1\,GF}\right)}{D+47.60} \qquad (4.2)$$

where D is the 8-bit digital reading of the voltage V_{out} given as $D = \dfrac{255}{2.25}V_{out}$.

Since there are uncertainties in the electronic components and the sensor sensitivities, it is better to use curve fitting to fit the calibration data. The transfer function is of the form $y = \dfrac{a\,x+b}{x+c}$, where a, b and c are constants, x is the digital reading and the output y is the pressure in terms of kPa. Hence it is appropriate to use this rational function to curve fit the calibration data and compute the constants a, b and c, which are also called the calibration parameters.

Curve fitting is done by method of least squares, and this kind of rational function needs non-linear least squares method to compute the parameters. Fortunately, Matlab's Curve Fitting Toolbox™ provides an in-built function called **fit()**, which computes the parameters using non-linear least squares method. The input arguments to the function are the measured calibration data and the fitting function model. The instruction was **fres = fit (vtg, pres, 'rat11')**, where **vtg** and **pres** are the digital reading and the pressure vectors, and **'rat11'** specifies the fitting function model; the output of the instruction is **fres** which contains the parameters a, b and c. Using these calibration parameters, the calibration curve was generated and is as shown is figure 4.3. This curve was used to characterize the sensor element. The following section will discuss the characteristics of the system with respect to a single sensor element.

4.2. Characteristics of the single sensor element system

Few loading experiments were performed on the single sensor element and the measurements were characterized by a few measures. This section contains the discussions of those measures.
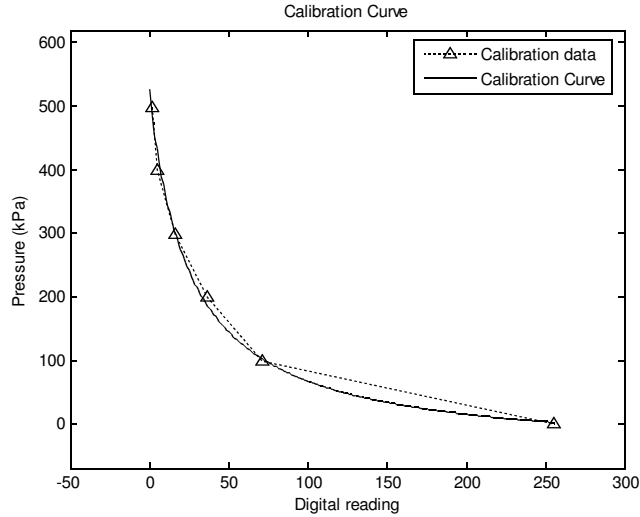
Figure 4.3. Calibration curve

4.2.1. Span and full-scale output

The span of the system is the dynamic range of the input that will be applied. The input here is the pressure. According to the Tekscan's specifications [27], F-Scan sensor has a span of 0-1034 kPa. However, the response of our system shows that the system saturates at about 503 kPa. Hence the span of this system is 0-503 kPa. And the output of the system is the voltage which is digitized by 8-bit ADC. The full scale output is 0-2.25 V or 0-255 digital reading. The range of the measurement system is affected by the sensitivity of the system. The sensitivity can be changed by changing the R1 resistance in the interface circuit in figure 3.3. By reducing the resistance, the threshold increases and the upper applicable input pressure increases. With the current setting, the minimum pressure that can change the output from 255 to 254 digital reading is about 4 kPa.

4.2.2. Accuracy of single sensor and spatial accuracy

The accuracy is specified in terms of inaccuracy or more generally by uncertainty. The various evaluations of the F-Scan system [5, 9, 13] say that it is not an accurate sensor and that the accuracies vary at different loads. Keeping this in mind, the data were collected for different loads and the experiment involved loading only a small part of the sensor area. The rubber pegs were used again for this experiment. The loading was done by placing the tiles. The pressure exerted was from 0-276 kPa and the readings for three sensor elements were recorded. The figure 4.4 shows the deviation of the readings from the actual pressure for three neighboring sensor elements. The maximum deviation was about ±44.8 kPa for all the three sensor elements. At the low pressures and the mid-pressures of 172-241 kPa, the sensor is more accurate. The assumption that all the sensors behave similarly does not however hold good, the maximum standard deviation of the pressure readings at the three sensor elements was about 16.4 kPa at input pressure of 184.7 kPa. Since the deviation is less than 10% of the actual pressure, there can be a compromise on this accuracy. Although the quantization error is high with just 8-bits, but we can now see the tradeoff.
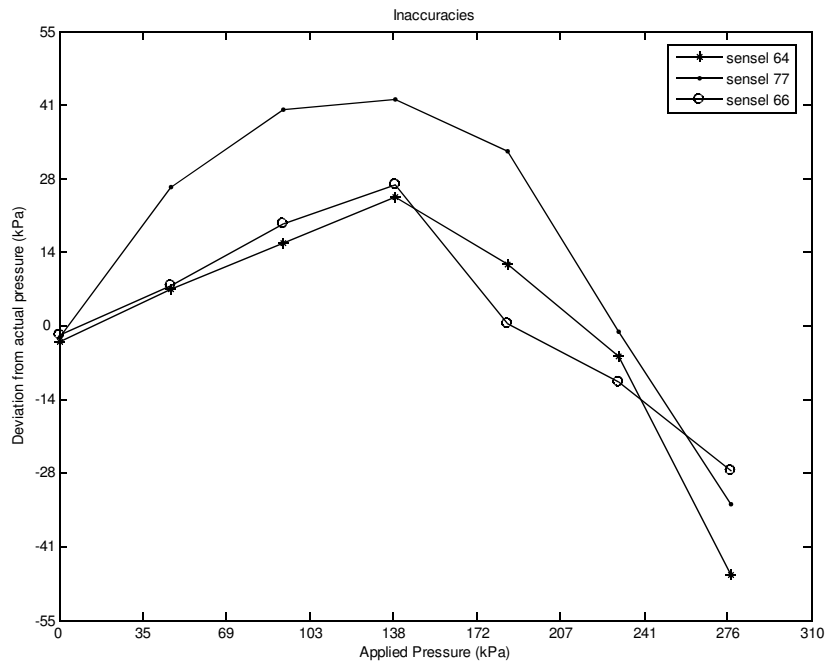
Figure 4.4. Inaccuracies in the sensor readings for application of pressure from 0-276 kPa
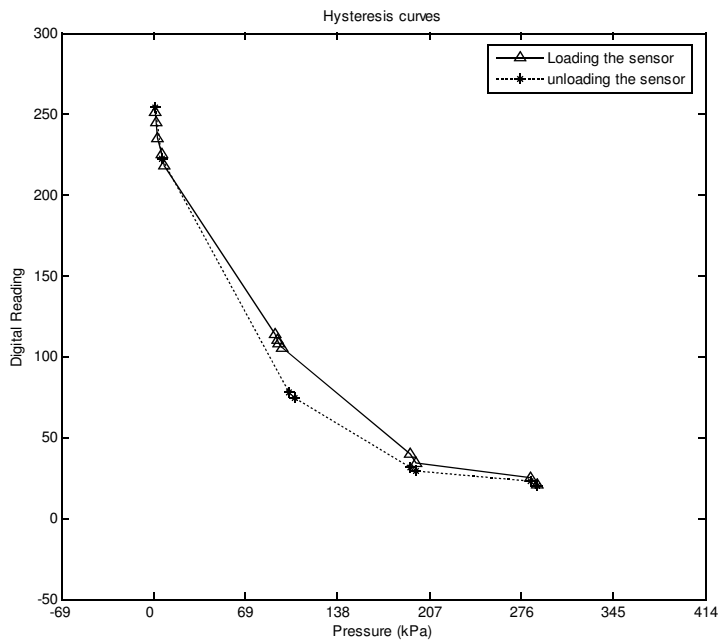
4.2.3. Hysteresis

Figure 4.5. Hysteresis curve

The sensor shows a tolerable amount of hysteresis. The hysteresis was measured for pressures in the range of 0-276 kPa. The loads were not exactly the same during the

loading and unloading cycle. A large hysteresis was shown between 69-207 kPa and the maximum amount was about 20 digital reading or 0.17 V which is about 7.5% of full scale output. Again the hysteresis is tolerable for not very precise measurements. This was static loading, but during dynamic loading conditions, the hysteresis characteristics may differ and can be worse [2].

4.2.4. Dynamic response

The dynamic response of the measurement mainly depends on the sensor, and the delays caused by the whole data acquisition system during A/D conversion, and transmission of the data to the PC. The dynamic response of the sensor is more important to be analyzed since the delays can be taken care of by more expensive electronics. The dynamic response of the sensor was recorded by giving a step input on a sensor element. The peg was placed on the element area and a dead weight of 50 gm was dropped from a height of about 3 mm over the peg. Although there would have been some bouncing of the dead weight, but not very considerable. The rise dynamics of the sensor element were recorded. The rise time as seen from the figure 4.6, is about 1.24 ms. The dynamics of the sensor element were also measured for decay by just lifting the dead weight off the peg. The decay time was also 1.24 ms. By observing the dynamic profiles of rise and decay, we can see that there is a slight difference. The reason for this difference is the hysteresis. Also, the step input during loading was not a perfect step, hence we see a larger overshoot in rise dynamics.
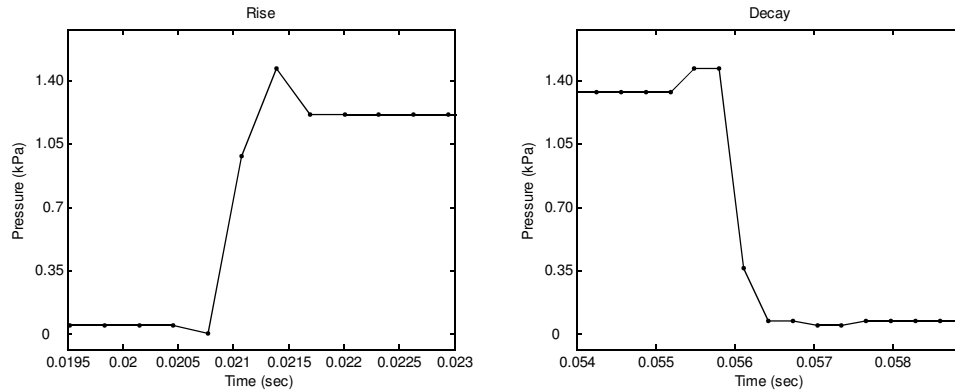

Figure 4.6. Dynamic response for step input

Another experiment that was done was ball impact experiment. A rubber ball weighing about 150 gm was dropped twice from heights of 250 mm and 100 mm on the sensor element and the responses of the sensor were recorded. Figure 4.7 displays the response. We see that the profile obeys the law, that the force or pressure curves vary sinusoidally with time during the period of contact of the ball with the surface. The time period of the contact of the ball with the surface remains the same irrespective of the height it is dropped from. This can be seen distinctly, that the contact time in both the cases is 4 ms. Also the rise and fall profiles in both the 250 mm and 100 mm cases are quite similar except for slight difference at the lower pressures during the fall. This difference can be again attributed to hysteresis. The ball impact experiment gives a clearer picture of

dynamic response of the sensor element, because, during the dead weight dropping experiment, the loading step input was not perfect and thus it gave different dynamic profile than the unloading profile. But in the case of ball impact experiment, the natural dynamics of the elastic collision can be considered. This gives a higher level of confidence about the dynamic characteristics of the sensor element.
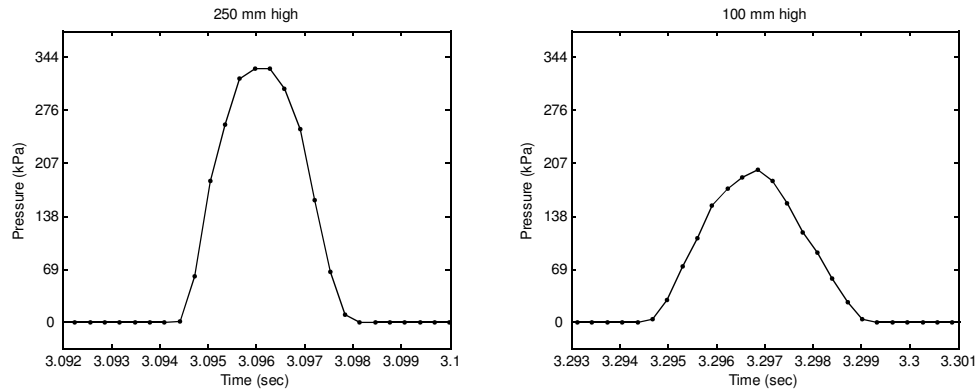

Figure 4.7. Dynamic response for ball impact dropped from 250 mm and 100 mm high

When looking at the complete measurement system, as discussed earlier in this section, the delays caused by data acquisition components hinder the dynamic characteristics. And the scanning time of our system is 300 ms per scan of a single foot. This discourages the use of the system for dynamic measurements, but a ray of hope is seen when the scanning can be done smartly and sparsely, losing some spatial resolution and then reconstructing the pressure map intelligently.

4.2.5. Effect of loading a sensor element on neighborhood

The method of construction of the sensor, has given rise to various problems such as hysteresis, inaccuracies, and so on. Another bad effect is the effect of loading one sensor element, on the neighboring sensor elements which share either the same row or same column. Figure 4.8, shows the effect. The experiment done, was by placing the peg on a sensor element and it was loaded. The responses of the neighboring three elements on all the sides were also recorded. The center element is the one that was loaded, but the neighboring elements also showed some response. Four different pressures of 503 kPa, 414 kPa, 214 kPa and 110 kPa were exerted. In each case the maximum erroneous pressures shown by any of the neighboring sensor element were 61.3 kPa, 53.7 kPa, 31.0 kPa and 21.4 kPa respectively. Considering the errors as percentage of the input pressure we would see them as 12.2%, 13.0%, 14.5%, and 19.4%. So at lower pressures, the errors are higher and care has to be taken while using it for applications where the ground reaction forces would be computed from the pressure measurements, since the actual area of contact would be less but the amount of area affected as shown by the pressure maps would be higher. When sparse scanning is done these effects can be overcome, since, as the distance from the target element increases, the erroneous effect decreases.
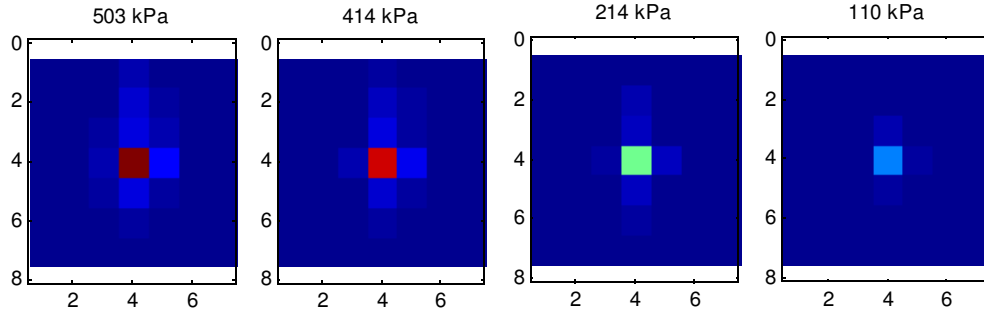
Figure 4.8. Effect of loading a sensel on its neighbors, at different pressures

4.3. Calibration of complete sensor

It was possible to discuss only a few characteristics of the sensor element because of the context in which we are going to use the system; it will not be used for high precision measurements, and it is not possible to take all the internal effects into consideration. There is a high chance of propagation of errors at every stage. So there is a need for end-to-end calibration of the complete sensor. All the sensor elements have to be loaded as uniformly as possible upto a certain range and then calibration parameters for each sensor element has to be computed.

4.3.1. Loading the sensor wholly

The total area of the sensor film is 21.9×10^3 mm² and to exert 503 kPa of pressure on the complete sensor film, there is need for 1124 kg of dead weight. Hence the sensor area was divided into three regions as shown in figure 4.9, using a rectangular base of area 12.9×10^3 mm², this reduced the need for dead weight to about 650 kg. The rectangular base was made of plexiglass, with rubber sheet on one side. This side faced the sensor film due to the requirement of soft surface. Then the base was loaded with ceramic tiles (each tile was 1.57 kg) and two lead bricks of 6 kg and 12 kg as dead weights. However, after loading beyond 57 kg, the system showed lot of noise in the output. And this noise was due to the fact that about 400 sensor elements were showing low resistance, and the average current that was drawn from the multiplexers was higher than their ratings. Therefore the range of pressures applied were only 0-45 kPa.

4.3.2. Computing the calibration parameters of the whole sensor

As already discussed in section 4.1.2, the calibration of an individual sensor element is done by fitting a rational function of form $y = \dfrac{a\,x+b}{x+c}$, to the calibration data and using the calibration parameters a, b and c for computing the pressures from the digital readings. In the same manner, the calibration parameters a_i, b_i and c_i were computed for i^{th} sensor element, where $i = 1$ to N; N is the number of sensor elements. As long as there is enough memory, storing 3N floating point numbers will not be a problem and computation of pressure from the digital reading using these parameters is also not computationally intensive, thus making it suitable for real time operation.
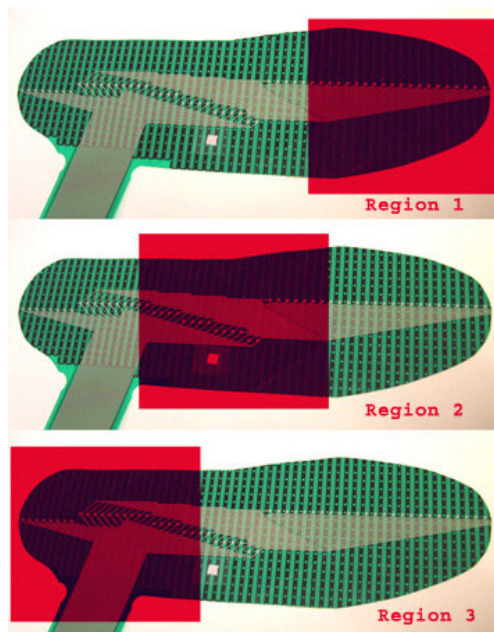
Figure 4.9. Application of region based, uniform loading on sensor film

4.3.3. Characteristics of the whole system

With the calibration of the complete sensor, the span of the sensor has reduced to 0-45 kPa, from 0-503 kPa. However this range is adequate for initial phases of usage of the system for our research purpose.

The problems of spatial accuracy or variations among the sensor elements, are solved since each sensor is now calibrated individually. However the issues of accuracy of the sensor, and hysteresis still persist.

The dynamic response, is now the dynamic response of the whole system. And as discussed in the previous sections, the time lag shown by the system is about 300 ms due to the limitations in the speeds of microcontroller board, and microcontroller to PC serial communication delays. Hence, the dynamic measurements conforming to the time response of the whole system, can be made.

4.4. Spatial filtering of the pressure map

Until now, we have seen a lot about the magnitude of the pressure measurements. The measurements that will be done using this system, would be giving two dimensional map of the pressure distribution, on the surface area of the contact of foot and ground. The left side figures in 4.10 and 4.11 show the unfiltered pressure distribution map. The pressures do not seem to be smoothly varying, because of the differences in sensitivities of the sensor elements. If the maps will be used for statistical data analysis, then it is required to have clean and smoothly varying data rather than noisy and discontinuous data. Hence

there is a need for spatial filtering of the pressure map after measurement. The widely accepted representation of the distributions is Gaussian. And also the simplest and fast filtering could be done by using Gaussian filtering. Hence a 3x3 kernel with σ = 1, given by the below matrix was used.

$$G = \begin{bmatrix} 0.0751 & 0.1238 & 0.0751 \\ 0.1238 & 0.2042 & 0.1238 \\ 0.0751 & 0.1238 & 0.0751 \end{bmatrix} \quad (4.3)$$

This matrix G is convolved with the pressure map using the Matlab function conv2. The effects of Gaussian filtering are smoothening of the image or the map and also blurring or degradation in the pixel values or in our case it is attenuation of the pressure values. In the case shown in the figure 4.11, the maximum attenuation is by 50%, but the pattern of the distribution has not changed much. Hence filtering is recommended for analysis of the distribution only and not for analysis of the pressure magnitudes.
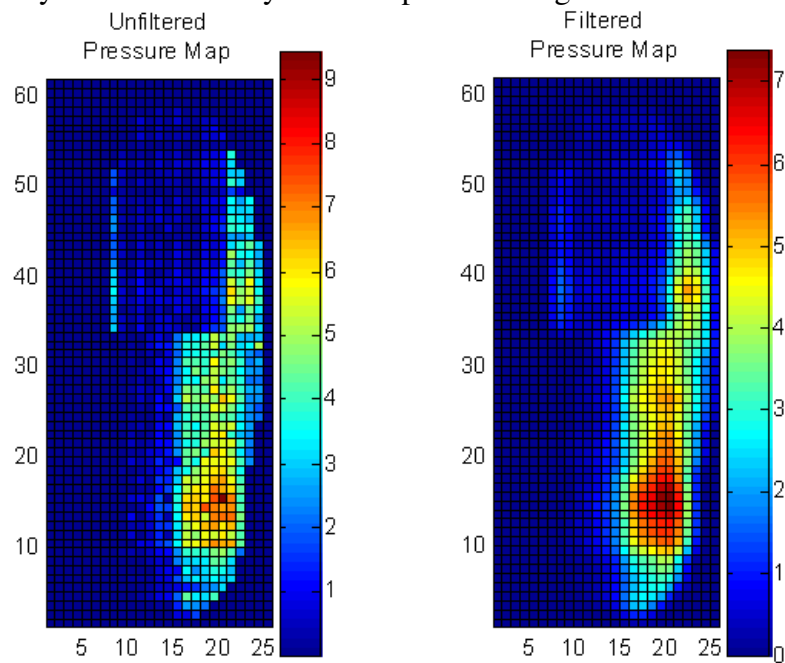

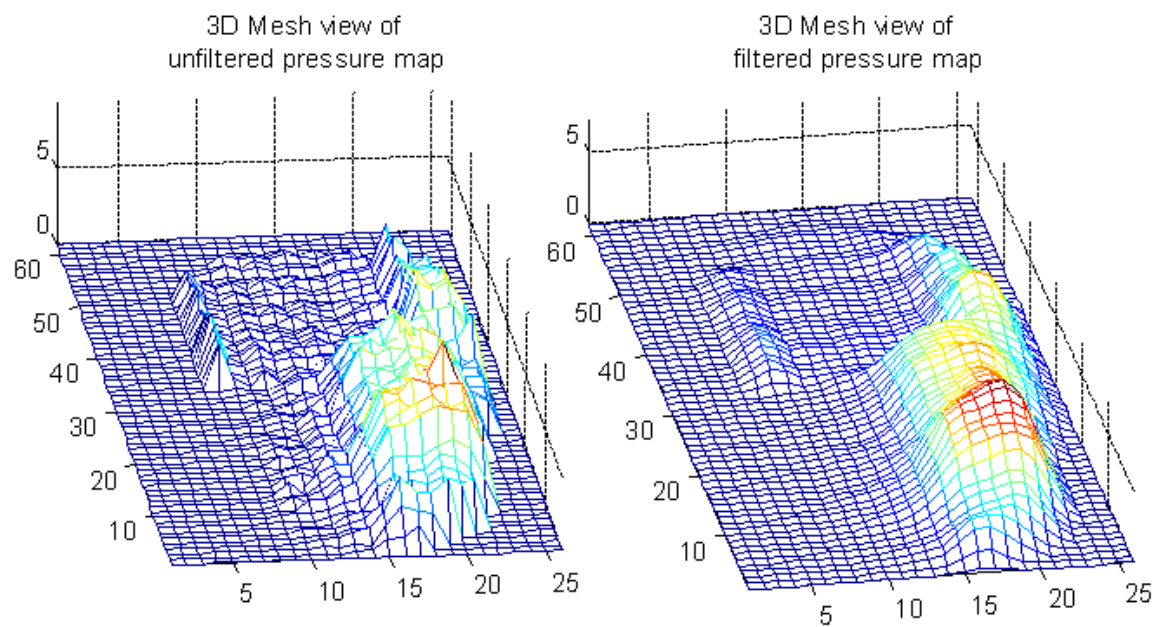Figure 4.10. Comparison of the unfiltered and filtered pressure maps

Figure 4.11. 3D Mesh views of the unfiltered and the filtered pressure map

5. Simulation of loading on the foot

The apparatus is now fully ready for application. A few experiments were conducted on the apparatus, by simulating the loading that happens in the foot of the humans or the robots. The section will give an idea about the method of simulation and analysis done to interpret the pressure maps.

5.1. Testing the apparatus

This section describes the experiments that were conducted to simulate the loading under the foot. Starting with, why is it necessary to simulate, follows the implementation of the simulation and then the experiments conducted using the simulating equipment.

5.1.1. Design rationale

Referring back to sections 1.1 and 1.2, we see that the factors affecting the foot pressures are the structure of the foot, structure of the ground, posture of foot striking the ground, dynamics of the striking, and also the weight of the human or the robot that exerts a force on the knee and affects the foot pressures. To test the equipment for all the cases in controlled environment with humans or robots walking, there is a need for sophisticated instrumentation like, motion capture, and other equipments. That is why it is necessary to artificially create these conditions. Here is an attempt made to simulate the loading on the knee, and how the loading on the knee affects the foot pressures is being studied. The force that the knee usually encounters when the human is standing on single leg is the weight of the whole body itself and hence the pressure maps change with change in the weight of the human or the robot. Also the pressure distribution changes when the orientation of the lower leg about the ankle joint changes or when the body sways about the ankle joint.

5.1.2. Implementation of the loading simulation

This section discusses two issues. One is the design of the artificial leg, and the second is the design of the loading system. The artificial leg that was made was very simple, made of wood. The tibial or the lower leg was just a wooden stick of length 432 mm and diameter of 31.75 mm. The foot was also made of wood, in the shape of human foot, of dimensions same as that of the sensor film, and to the sole was attached an in-shoe cushion. This was used to make the surface soft. The leg was attached to the foot using two L-shaped mounting brackets made of softer metal, so that the joint has some compliance. The leg was attached to the foot, towards the heel as it is in the real ankle. The sensor was sandwiched between the foot and a sole of an old shoe. Figure 5.1 shows the picture of the leg with sensor.

The leg was loaded using a scheme developed using simple pulleys, rope and dead weights. The design of the scheme is as shown in figure 5.3. A wooden frame was made and the pulley system was fit inside the frame, and the leg placed at the center of the

frame. A teflon hemispherical cylinder with a groove in it was fit on top of the knee, to reduce friction of the rope sliding over the knee. The figure 5.2 shows the picture of this experimental setup. The dead weight W in lbs, was placed and the force that was actually experienced by the leg at the knee was Fb given by

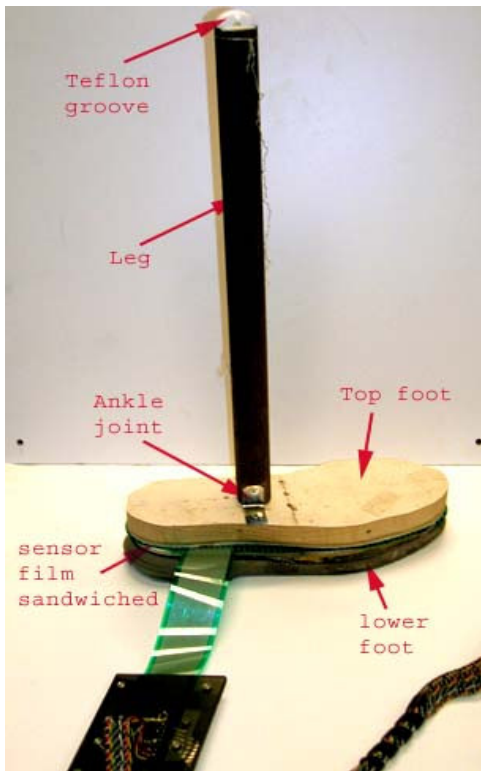$$Fb = 4W.cos(20^o) + 4W.cos(25^o) \approx 7.4W \qquad (5.1)$$

Figure 5.1. Picture of the artificial leg

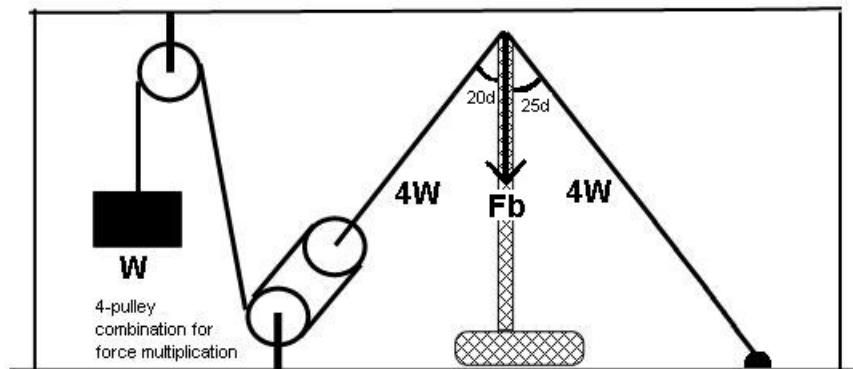Figure 5.2. Picture of the experimental setup

Figure 5.3. Pulley system for loading the artificial leg

5.1.3. Weight testing

Considering the lower strengths of the wooden frame and the rope which bore the tension, lower loads of W were applied. The loading was done by jars of nuts, bolts and screws each weighing 0.9 kg, 1.13 kg, and 0.9 kg respectively. Hence maximum W was 2.93 kg which exerted a force of about 214 N on the leg. Figure 5.4 shows the pressure maps obtained for three different loadings on the leg at 67 N, 147 N and 214 N. The colorbar shows the intensity of the pressures. This indicates the change and the distribution that is taking place under this simulated foot. The absence of the foot arch or the mid-foot region has made the pressure to be distributed completely near the hind-foot or the heel region. However there is always a scope for near reality simulations with better foot design.
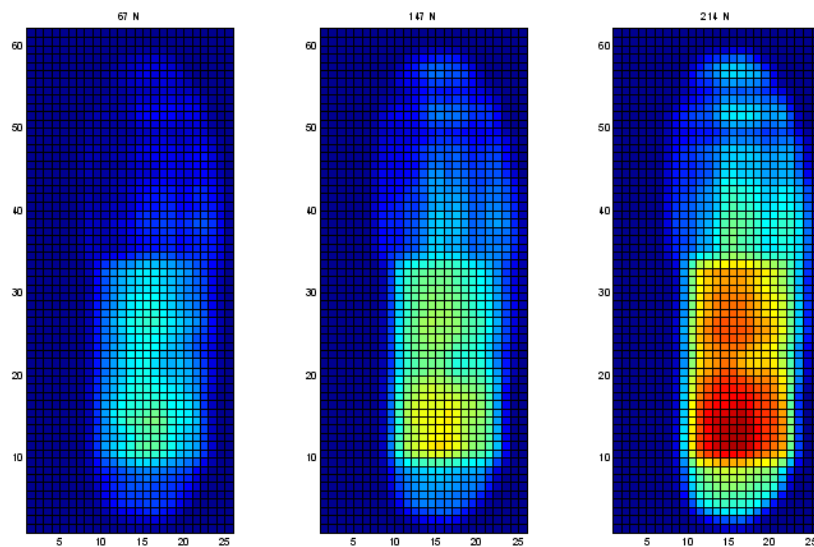

Figure 5.4. Pressure maps at 67 N, 147 N and 214 N on the leg

The other experiment that was done with the loading was to simulate the sways. Although sways are more dynamic, the pressure maps at the extremes of the sway positions were simulated. The right, left, anterior and posterior sways were forced on the leg. The figure 5.5, shows the pressure maps recorded for the sways and also the differences of those maps from initial condition. The leg was loaded with 67 N and there were sways forced on the leg. The amount of sways in terms of the angular displacement of the leg were, 3.6° on the right and 3.6° on the left and 7.3° in the anterior and 6.0° in the posterior directions.

The leg was also subjected to dynamic loading. The method used for dynamic loading was a dynamic right sway forced by a stepper motor running at a speed of about 4.5 RPM, thus swaying the leg at an angular displacement of 0.33 deg/sec. Although due to low scanning speed of about 3 foot scans per second, smaller transients could not be captured. Figure 5.6, shows the picture of the setup and figure 5.7, displays the difference of sequence of ten continuous scans from the initial condition, while the dynamic right sway was going on. With all these experiments conducted, data was collected and now analysis of the data is discussed in the next section.
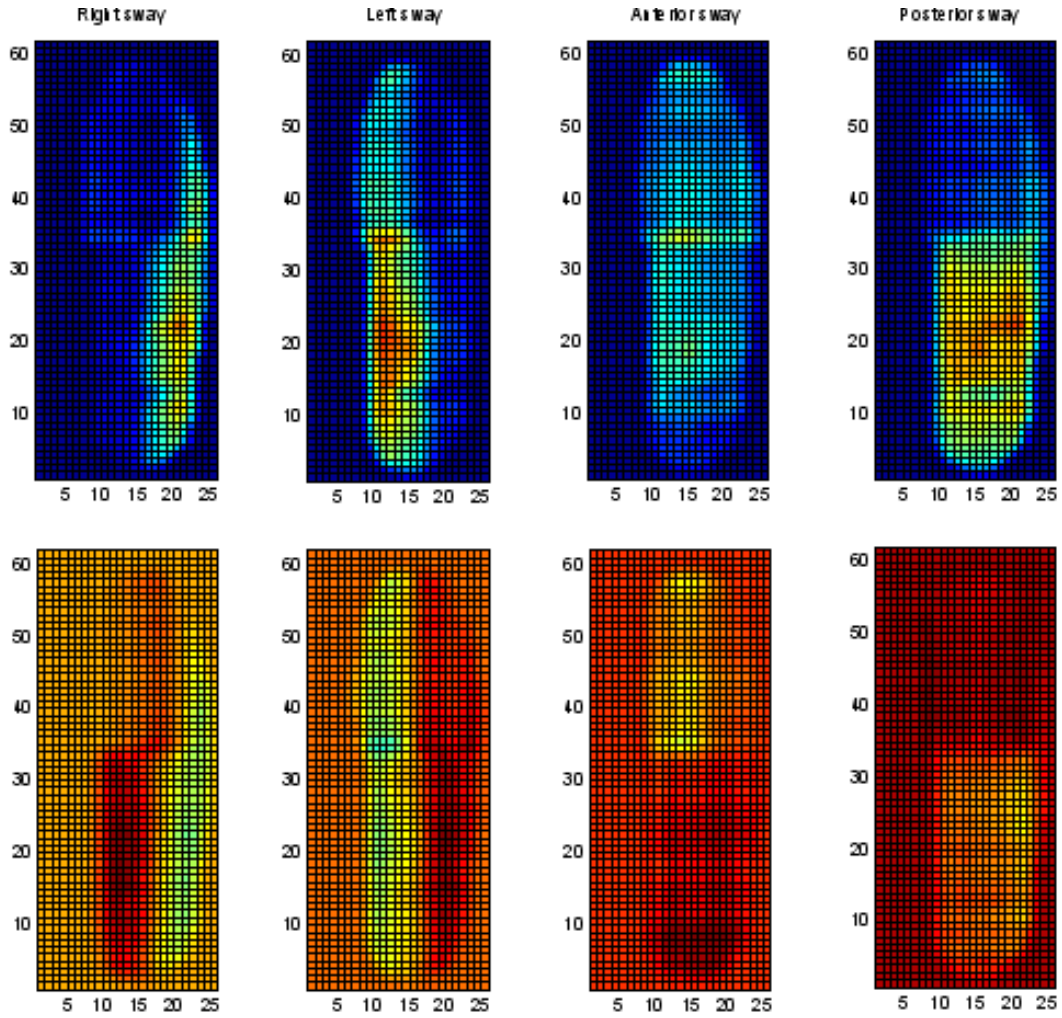
Figure 5.5. Pressure maps for right, left, anterior and posterior sways on the leg
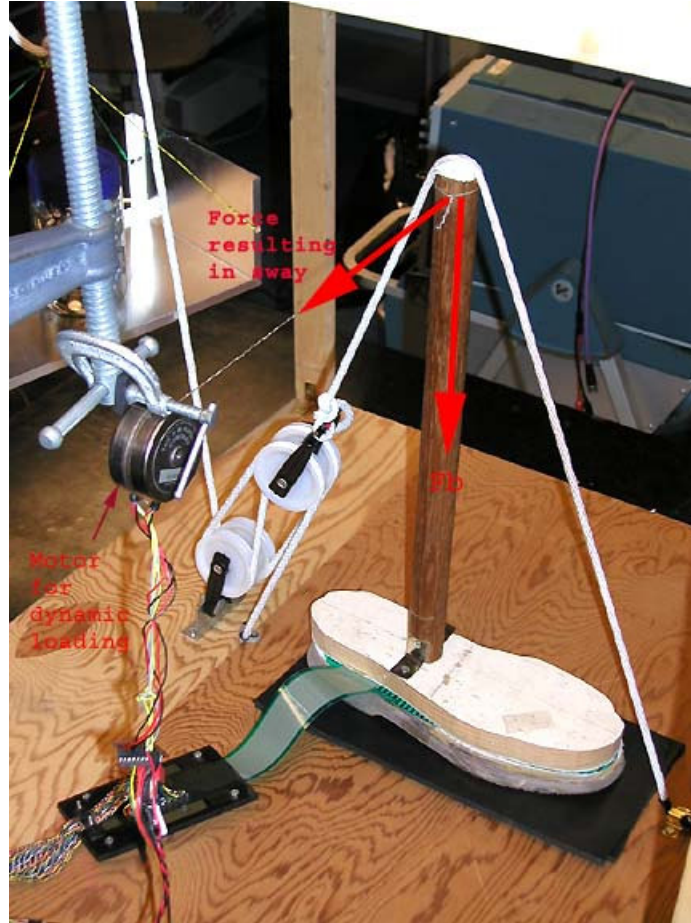
Figure 5.6. Setup for dynamic loading. The stepper motor forces a sway on the leg.

5.2. Analysis of the pressure map using method of moments

In the section 4.3, we saw that after filtering the pressure map, it was a smooth pressure distribution on the two dimensional surface. All the natural distributions behave according to the Gaussian form. And hence analyzing even these pressure distributions as Gaussian would make it easier to interpret for different cases. It was seen in the previous section of 5.1, that most of the maps were unimodal and there was central tendency occurring at high pressure regions. So, for representing all this data which cluster around the high pressure region, we have used the method of moments [19]. The distribution was analyzed by computing the first, second and third moments. The general expression for computing the nth moment is given by

$$\boldsymbol{\mu_n} = \frac{\sum_{i=1}^{N} (\mathbf{x_i} - \boldsymbol{\mu_1})^n P_i}{\sum_{i=1}^{N} P_i} \qquad (5.2)$$
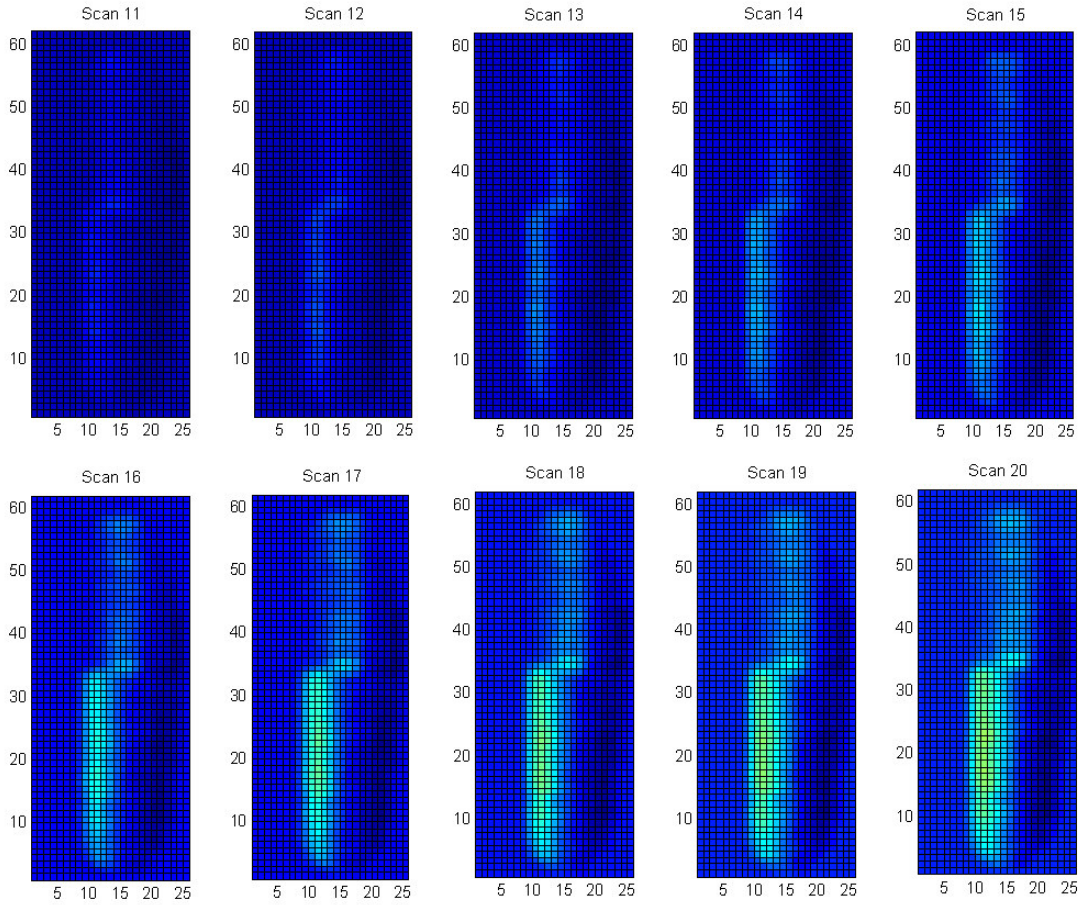
45

Figure 5.7. Sequence of pressure maps captured for dynamic right sway on the leg at a rate of 0.33 deg/sec

where

$$\boldsymbol{\mu_1} = \frac{\displaystyle\sum_{i=1}^{N} \mathbf{x_i} P_i}{\displaystyle\sum_{i=1}^{N} P_i} \qquad (5.3)$$

Here, considering N discrete points, with i^{th} position described by the 2D vector $\mathbf{x_i}$, the pressure value at that point is described by P_i. The discrete elements are the sensor elements and in our case N=824. The position vector as considered in our case was in pixel units. It is possible to convert them into engineering units, given that it is possible to measure the exact locations of the elements on the sensor film without introducing errors. An approximate distance between two consecutive elements is 5.08 mm.

1st Moment:
The first moment is nothing but the mean of the distribution or in physical terms it is the Center of Pressure (COP) of the pressure distribution. Equation 5.3, is used to compute the COP. According to [20, 21], COP is the point which corresponds to the Zero Moment

Point or the point where bending moment due to ground reaction forces or inertial effects is zero. The authors of [16] have also used the COP as a measure to do balance testing of the humans. The COP reflects the movement of center of gravity, which gives the information about the stability of the human or the robot. Hence computation of this parameter is an essential component of pressure map analysis.

2nd Moment:
The second moment specifies the variance and its square root, the standard deviation of the data points around the mean or COP of the distribution. The variance is computed by equation 5.4, and σ is the standard deviation of the distribution. The standard deviation of the distribution defines the spread of the stresses or the pressures around the high pressure regions. Higher the standard deviation, higher is the spread. When the standard deviation is lower, the pressures are concentrated in a particular region and they stress out the region a lot. So use of standard deviation is necessary for assessment of the stresses on the foot.

$$\sigma^2 = \mu_2 = \frac{\sum_{i=1}^{N}(\mathbf{x_i} - \boldsymbol{\mu_1})^2 P_i}{\sum_{i=1}^{N} P_i} \qquad (5.4)$$

3rd Moment:
Skewness is the measure dependent on 3rd moment. The third moment is given by equation 5.5, and skewness is defined by equation 5.6.

$$\mu_3 = \frac{\sum_{i=1}^{N}(\mathbf{x_i} - \boldsymbol{\mu_1})^3 P_i}{\sum_{i=1}^{N} P_i} \qquad (5.5)$$

and

$$Skewness = \frac{\mu_3}{\mu_2^{3/2}} \qquad (5.6)$$

Skewness gives an idea about the asymmetry of the distribution around its mean. The figure 5.8, shows the structure of two differently asymmetric curves. The curve having a 'tail' towards the positive axis has a positive skewness and the one having an asymmetry towards negative axis has negative skewness. The skewness is a non-dimensional quantity, and it specifies only the measure of asymmetry. In case of 2D data, the skewness measure gives asymmetry along the x and the y axes. In the pressure distributions under the foot, we can see that, when the distributions have an asymmetry around the COP, the leg tends to tip over towards the opposite side of the tail and hence the control algorithm has to be able to correct the posture of standing so that the skewness is inside the "safe limits" or the magnitude of skewness is low.
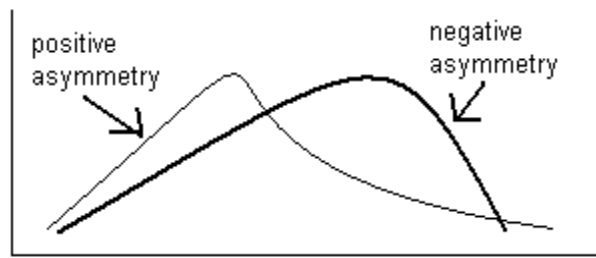
Figure 5.8. Illustration of the asymmetry in the curves

The three statistical measures of COP, standard deviation and skewness provide the necessary information about the pressure distribution under the foot. Higher moments may prove useful in the future, but at this preliminary stage the first three moments seem adequate for building more intuition. The next section uses these measures to analyze the data measured from the sway experiments.

5.3. Static sways and their analyses

As already described about the sway experiments, right, left, anterior and posterior sways by magnitudes of 3.6° on right and left, 7.3° on anterior and 6.0° on posterior sides. The analysis of each case was done with respect to the initial zero-sway condition. The figure 5.9 shows all the sways and table 5.1 shows the COP, standard deviation and skewness measures for all the cases. The numbers explaining the measures in the table, for the four sway cases are difference of those from the measures of initial condition. And the figure 5.9, also shows the difference of pressure maps of sways from the initial condition.
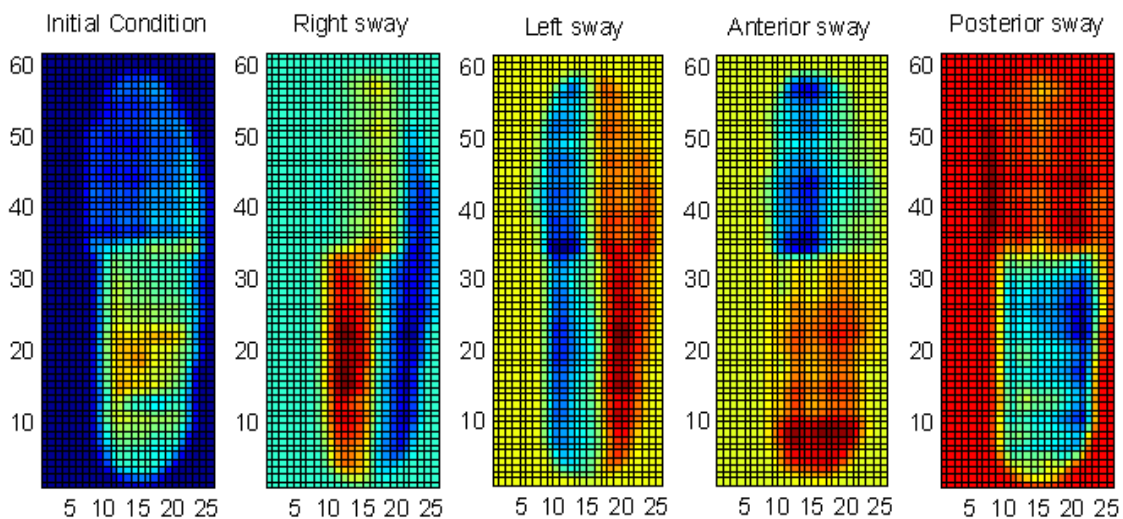

Figure 5.9. Pressure maps of initial condition, right, left, anterior and posterior sways

Parameters (pixel units)	Initial Condition		Right sway by 3.6°		Left sway by 3.6°		Anterior sway by 7.3°		Posterior sway by 6.0°	
	X axis	Y axis	X axis	Y axis	X axis	Y axis	X axis	Y axis	X axis	Y axis
COP	14.75	19.50	4.39	2.53	-3.49	4.72	-0.43	10.96	0.31	-0.50
Std.dev.	3.56	8.78	-1.45	1.90	-1.28	4.78	-0.05	3.20	0.34	0.01
Skewness	0.11	0.06	-0.30	0.17	0.17	0.40	0.24	0.20	-0.10	-0.08
Peak Pres.	14.8 kPa		20.6 kPa		22.5 kPa		16 kPa		22.2 kPa	

Table 5.1. COP, standard deviation, skewness and peak pressure for all the sways and initial condition

Comparing the COP displacement from the initial condition, in all the cases there is a considerable displacement, but it is not very large for posterior sway. The amount of spread or the standard deviation is also distinctly changing except for the posterior sway. We also see that the spread decreases deeply along x-axis for the right sway and also that the right edge of the foot is experiencing high stress. Looking at the asymmetry, the skewness is least for anterior sway, and very high in positive y-axis for posterior sway and very high in negative x-axis for right sway. The peak pressures are also higher for the right sway and posterior sways. And hence more stable and low stress postures are left and anterior sways for the right foot. In the case of left foot, the right and left sways would interchange, but the anterior and posterior sway result would remain same.

5.4. Dynamic loading simulations

The section 5.1.3 has described a method for generating dynamic loading on the leg. And this loading is nothing but a dynamic sway on the right side. The scheme was to sway the leg at a speed of 0.33 deg/sec and then revert it back to its original state. The speed of the sway was slow due to the constraints in scanning speeds. This experiment was conducted only to demonstrate the dynamic scanning and that a simple analysis could be done using the method as described in section 5.2. There were two sets of data. One set was sway when the leg was loaded with 67 N and other when leg was loaded with 214 N. The figure 5.10, shows the plots of the COP analysis of the dynamic data on both the sets. In the top figure showing the COP trajectories, we see that the initial condition and the end condition are far from each other in 67 N case than in 214 N case. This is certainly due to the hysteresis shown during dynamic loading. We see that the hysteresis is less in higher loading case. But taking a look at the Euclidean distance profile, which explains the distance of the COP at that instance of time from the initial condition, the transition of COP is smoother in lower loading. And in the plots of angular displacement of the COP from initial condition, profile for lower load shows no displacement for a long time, but then it starts displacing while the leg is returning back from sway.
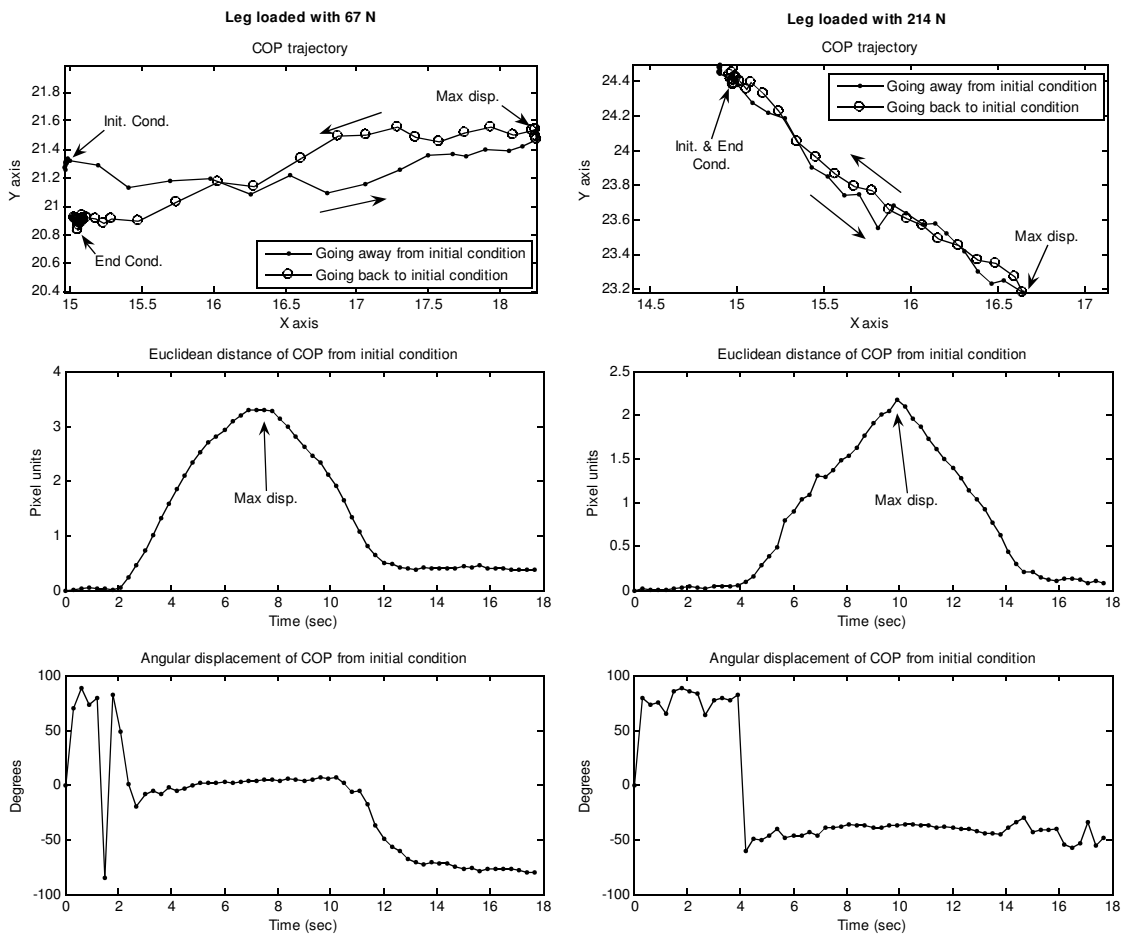
Figure 5.10. Movement of COP, euclidean distance and direction of movement, left side plots are for 67 N loading on leg and right side plots are for 214 N loading

Now, taking a look at the standard deviation or the spread of distribution and the skewness measures in figure 5.11, the spread is distinctly seen in both the x and y directions for lower loading case. But for higher loading the spread is less in the x direction, but is high in the y direction. The same is with the skewness measure. The skewness for initial conditions in x direction for both lower and higher loading cases, is low, but it increases as the displacement increases. Even in these measures, the hysteresis is clearly seen for lower loading case, but it is very less for higher loading case. Hence the uncertainties in pressure maps decrease with increase in loading.
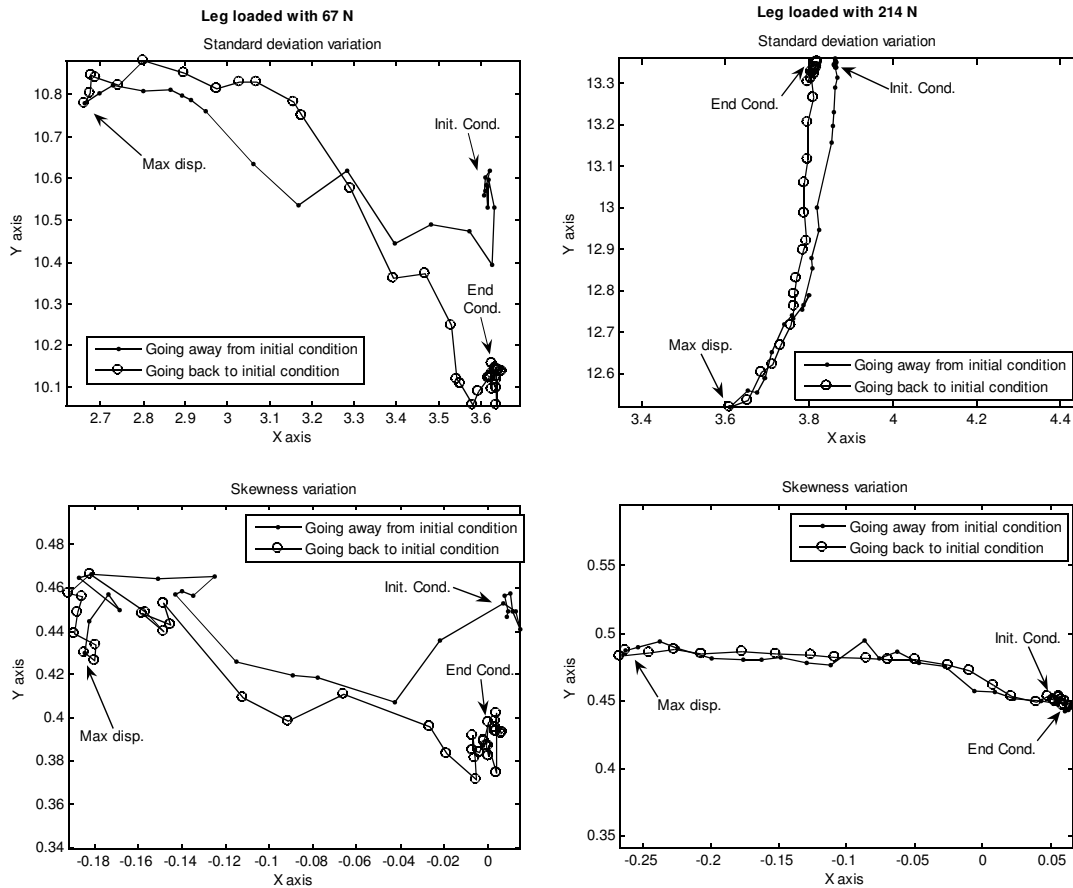
50

Figure 5.11. Variation in standard deviation and skewness along x and y axes, left side plots are for 67 N loading on leg and right side plots are for 214 N loading

5.5. Sequence and rationale of future experiments

The experiments carried out until now, have been focused more on the sways of the leg on all the sides. There is a lot of scope in experimenting with the walking and running in humans or artificial legs. The heel strike and toe off timings, impact dynamics, and the rolling foot contours are interesting to study. There is also scope for experimenting with different ground terrains and identifying the surface texture. These would be used for development of customized control laws for different surfaces. In the analysis part, the 4th moment or the kurtosis can be computed and analyzed for getting more information on the shape of the distribution. However these analysis methods might have to be modified when the pressure maps become multimodal like in the case of human foot. Relationships can be established between the statistical measures described here and the state variables of the dynamic system of walking robots thus leading to intelligent control in robots.

6. Summary of the work

In the introductory section, we have seen what are the factors influencing the foot pressure maps, and also what are the characteristics of the foot pressure maps. The structure of the feet, ground, static and dynamic postures of the foot while standing or walking and the kinetics of placement of the foot, all generate distinct pressure distributions. In the robotic applications, the dynamic walking needs a complete information about the foot pressure distributions and their dynamics. The pressure maps can also be used to control the walking cycle and correct the disturbances caused during walking.

There were discussions about different measurement methods for plantar pressures. A deeper understanding of force sensitive resistors was highlighted, since the F-Scan sensor behaves similar to the FSR.

The F-Scan sensor is a thin, robust and simple resistive sensor for measurement of foot pressures. There are about 960 sensing elements on the sensor film, thus giving high spatial resolution. A survey about the evaluations by other researchers showed:
- F-Scan sensor is inaccurate
- The sensitivities of the sensor elements are inconsistent due to manufacturing drawbacks
- The plastic based material is deformable and experiences creeping problems
However, inspite all these problems, its simplicity, low costs, spatial resolution and thinness motivated us to use it for our research.

The measurand behavior was studied by applying pressures on an individual sensor element. Using this behavior, the interface electronics was designed. Considering the geometry and large density of sensing elements, the analog multiplexers were used to address the elements.

The multiplexers and interface electronics were interfaced to the Zilog-80 microcontroller board. The low level software was designed to have low time delays. The sensor addresses were sent to the digital ports for addressing the multiplexers and the ADC was used to digitize the signal from the sensor. The PC was communicating with the microcontroller, and the scanned data was transmitted to the PC. The routines for display and processing of the data were written on Matlab. The user interface displayed the pressure map of the foot.

The system was then calibrated by uniform loading on the sensor film, and the characteristics were measured. A first order rational function was used to curve fit the calibration data. The loading experiments were done on a single sensor element. The calibration data showed the span of 0-503 kPa for the single sensor. The inaccuracy was low for mid range of pressures. The sensor showed a high hysteresis for mid range of pressures of about 100-300 kPa. But the dynamic response of the element was motivating.

Complete sensor calibration was done for a small range of 0-45 kPa, due to problems with the electronics. And then the pressure maps were filtered spatially to attain smooth

transitions between the pixels.

The system was evaluated by simulating the pressure distributions for different cases. A pulley based simulation frame, an artificial leg were built and experiments with sways were conducted. Static and dynamic sways were forced on the artificial leg. The measured pressure maps were analyzed using moments and the center of pressure, standard deviation and skewness measures were computed for each cases and the results were interpreted. The same measures were computed for a dynamic sway experiment also.

In conclusion, this work showed a different way to measure foot pressures, for artificial leg. The method of analysis used was also a good component of the package. Although there were many defects in the system especially pertaining to the electronics, like, the delays, low resolution of ADC, low current ratings of multiplexers, to name a few. But as an apparatus for initial phase of the research, it provides a good infrastructure for future research.

In the future, it would be feasible to experiment on using more realistic structure of the foot, more anthropomorphic, with compliance. This can give a better picture of the pressure distributions generated during dynamic walking. Analysing these pressure maps is a challenge and using those measurements for developing control algorithms for the joints of the leg is the target. Apart from this, another challenge is to analyse the pressure maps for different terrain textures, and with different kinetic conditions of the foot.

References

[1] S.J.Morris, A shoe-integrated sensor system for wireless gait analysis and real-time therapeutic feedback, a doctor of science thesis at MIT, June 2004.

[2] T.Sumiya, Y.Suzuki, T.Kasahara, H.Ogata, Sensing stability and dynamic response of the F-Scan in-shoe sensing system: A technical note, Jour. of Rehab. Res. & Dev., Vol. 35 No.2, June 1998, p 192-200

[3] Y.Tanimoto, H.Takechi, H.Nagahata, H.Yamamoto, The study of pressure distribution in sitting position on cushions for patient with SCI, IEEE Trans. on Instrumentation & Meas., vol 47, no.5, Oct 1998, p 1239-1243

[4] P.Sardain, G.Bessonnet, Gait analysis of a human walker wearing robot feet as shoes, Proc. of 2001 IEEE Int. Conf. on Rob. & Auto., May 2001, p 2285-2292

[5] J.Woodburn, P.S.Helliwell, Observations on the F-Scan in-shoe pressure measuring system, Clin. Biomech. vol. 12, No.3, 1997, p S16

[6] E.Morin, S.Reid, J.M.Eklund, H.Lay, Y.Lu, J.Stevenson, J.T.Bryant, Comparison of ground reaction forces measured with a force plate, F-Scan and multiple individual force sensors, Queen's Univ., Ontario, Canada.

[7] B.J.Fregly, W.G.Sawyer, Estimation of discretization errors in contact pressure measurements, Jour. of Biomech. 36 (2003) 609-613, Oct 2002

[8] F.Vecchi, C.Freschi, S.Micera, A.M.Sabatini, P.Dario, R.Sacchetti, Experiemental evaluation of two commercial force sensors for applications in biomechanics and motor control, 5th Ann. Conf. of Int. FES 2000.

[9] H.Hsiao, J.Guan, M.Weatherly, Accuracy and precision of two in-shoe pressure measurement systems, Ergonomics, 2002, vol.45, no.8, 537-555

[10] R.Verdejo, N.J.Mills, Heel-shoe interactions and the durability of EVA foam running-shoe midsoles, Jour. of. Biomech. 2004.

[11] H.Zhu, N.Maalej, J.G.Webster, W.J.Tompkins, P.B.Y.Rita, J.J.Wertsch, An umbilical data-acquisition system for measuring pressures between the foot and shoe, IEEE Trans. on Biomed. Engg. vol.37. no.9, sept 1990

[12] A.Goswami, Postural stability of biped robots and the foot-rotation indicator point, Int. Jour. of Rob. Res., vol 18, no.6, June 1999, pp. 523-533

[13] Z.P.Luo, L.J.Berglund, K.N.An, Validation of F-Scan pressure sensor system: A technical note, Jour. of Rehab. Res and Dev. vol.35, no.2, june 1998, pp.186-191

[14] S.Urry, Plantar pressure-measurement sensors, Meas.Sci.Technol.10(1999)R16-R32.

[15] R.E.Goddard, Y.F.Zheng, H.Hemami, Control of the heel-off to toe-off motion of a dynamic biped gait, IEEE Trans. on Sys. Man Cyb., vol.22, no.1, jan/feb 1992, pp.92-102

[16] T.Tanaka, H.Takeda, T.Izumi, S.Ino, T.Ifukube, Effects on the location of the center of gravity and the foot pressure contribution to standing balance associated with ageing, Ergonomics, 1999, vol.42, no.7, 997-1010

[17] M.Lowe, A.King, E.Lovett, T.Papakostas, Flexible tactile sensor technology: bringing haptics to life, Sensor review, vol 24, no.1, 2004, pp.33-36

[18] H.Tan, L.A.Slivosky, A.Pentland, A sensing chair using pressure distribution sensors, IEEE/ASME Tran. on Mechatronics, vol.6, no.3, sept 2001, pp.261-268.

[19] W.H.Press, Numerical recipes in C: the art of scientific computing, 1988-1992 Cambridge Univ. Press., Section 14.1, pp.610-615.

[20] P.Sardain, G.Bessonnet, Forces acting on a biped robot, center of pressure-zero moment point, IEEE Tran. on Sys. Man & Cyb. - Part A: Sys. & Humans, vol.34, no.5, sept 2004, pp.630-637

[21] P.Sardain, G.Bessonnet, Zero moment point-measurements from human walker wearing robot feet as shoes, IEEE Tran. on Sys. Man & Cyb. - Part A: Sys. & Humans, vol.34, no.5, sept 2004, pp.638-648.

[22] K.Hoffman, K.Decker, Influence of the measuring grid of a foil sensor on the accuracy of pressure measurements, Vienna Univ. of tech., Austria, 2003.

[23] T.Papakostas, J.Lima, M.Lowe, 5.3: A large area force sensor for smart skin applications, Sensors, 2002, Proc. of IEEE 2002.

[24] Single serial button, user's guide, Flexiforce, dec. 1998.

[25] J.Fraden, Handbook of modern sensors, 3/e AIP press, 2003.

[26] App. Note on Interfacing a pressure sensor with a Z8 encore! MCU, AN019501.

[27] Tekscan Inc., MA, URL: www.tekscan.com

[28] Hung Do PT, The human foot, Vanderbilt Sports Medicine.

[29] S.H.Collins, M.Wisse, A.Ruina, A three-dimensional passive-dynamic walking robot with two legs and knees, Int. Jour. Rob. Res. vol.20, no.7, July 2001, pp.607-615

[30] A.Prochazka, Comparison of natural and artifical control of movement, IEEE Tran. of Rehab. Engg, vol.1, no.1, mar 1993, pp.7-17.